

FATIGUE ENHANCEMENT OF CATEGORY E' DETAILS IN
STEEL BRIDGE GIRDERS USING CFRP MATERIALS

By

Benjamin N. Kaan

Submitted to the graduate degree program in Civil Engineering and the
Graduate Faculty of the University of Kansas School of Engineering
in partial fulfillment of the requirements for the degree of
Master of Science.

Dr. Caroline Bennett

Chairperson

Committee Members:

Dr. Ron Barrett-Gonzalez

Dr. Stan Rolfe

Date Defended: 12/14/2008

The Thesis Committee for Benjamin Kaan certifies that
this is the approved version of the following thesis:

FATIGUE ENHANCEMENT OF CATEGORY E' DETAILS IN
STEEL BRIDGE GIRDERS USING CFRP MATERIALS

Chairperson

Committee Members:

Date Defended: _____12/14/2008_____

ACKNOWLEDGMENTS

First I would like to thank Drs. Caroline Bennett, Ron Barrett, Stan Rolfe, and Adolfo Matamoros for their guidance, expertise, and enthusiasm on this research. I would also like to thank the University of Kansas Transportation Research Institute for providing the funds necessary to accomplish this project.

Additionally, I would like to thank Mr. Ron Bruce of Builder's Steel in Kansas City for his contribution of the materials and fabrication required for the steel specimens. I would also like to thank Jim Weaver for his assistance with the equipment in the structural laboratory at Learned Hall.

Finally, I would especially like to thank my wife, Kimberly, my son, Elijah, and my daughter, Stella, for their support and patience throughout this project.

ABSTRACT

Carbon Fiber Reinforced Polymer (CFRP) composite overlay elements were developed to improve the fatigue performance of Category E' steel details. By increasing the stiffness of the detail with the CFRP overlay, the stress demand at the weld is reduced, resulting in an increased fatigue life of the detail. The CFRP overlays were also designed to be tough enough to resist internal crack growth and delamination due to shear stress from applied loads. Development of the CFRP overlay elements is described, including material testing, finite element modeling of the composite overlay behavior, and a finite element parametric study to investigate relative effects of CFRP element properties. Fatigue testing of steel specimens stiffened with CFRP overlay elements is also described, with bond thickness between the steel and composite materials varied. Results showed that the CFRP elements are robust enough to resist both internal and bond degradation when tested at a stress range of 138 MPa (20 ksi), and can significantly extend the fatigue life of welded details. Modeling results showed that the stress range at the welded joint can be significantly reduced by application of the CFRP overlay element. While a good bond was maintained, crack initiation was effectively eliminated in coverplated specimens. Bond tenacity was investigated and recommendations for achieving good bond based on materials and thicknesses investigated are described.

TABLE OF CONTENTS

Acceptance Page	i
Acknowledgments	ii
Abstract	iii
Table of Contents	iv
List of Figures	vi
List of Tables	viii
List of Symbols	viii
 Chapter 1 – Introduction	
1.1 Research Objectives	1
1.2 Division of Research	1
 Chapter 2 – Background Information & Literature Review	
2.1 General Background Information	4
2.2 CFRP Materials	5
2.3 Literary Review of Previous Investigations Utilizing CFRP Materials for Fatigue Enhancement of Structural Steel	6
 Chapter 3 – CFRP Overlay Development	
3.1 Objective	11
3.2 Experimental Setup	11
3.2.1 Steel Specimens	12
3.2.2 CFRP Overlay Development	13
3.2.3 Fatigue Testing Experimental Setup	17
3.2.4 Finite Element Modeling Experimental Setup	20
3.3 Discussion of Results	23
3.3.1 Experimental Test Results	23
3.3.2 Finite Element Model Results	29
 Chapter 4 – Fatigue Enhancement Testing of CFRP Overlays	
4.1 Objective	34
4.2 Experimental Setup	34
4.2.1 Steel Specimens	35
4.2.2 CFRP Overlay Elements	36
4.2.3 CFRP-Stiffened Specimens	37
4.2.4 Fatigue Testing Experimental Setup	39
4.3 Discussion of Results	41
4.3.1 Effects of Bond Thickness on CFRP Overlay Effectiveness	44
4.3.2 Effects of Bond Characteristics on Frequency of Debonding	49

Chapter 5 – Conclusions and Recommendations	
5.1 Conclusions and Recommendations	51
References	54
Appendix A – Specimen Test Data	57
A1.1 Introduction	58
Appendix B – Instructions for Manufacture and Bonding of CFRP Overlays	64
B1.1 Instructions for Manufacture of CFRP Overlays	65
B1.1.1 Material Preparation	65
B1.1.2 CFRP Overlay Layup	66
B1.1.3 Post-Processing of CFRP Overlays	79
B1.2 Instructions for Bonding of CFRP Overlays	88
B1.2.1 Bonding of CFRP Overlay Elements	88
Appendix C – Supplemental Information	92
C1.1 CFRP Material Testing	93
C1.1.1 Experimental Setup	93
C1.1.2 Discussion of Results	94

LIST OF FIGURES

Figure 1-1.	General Research Procedure	2
Figure 3-1.	Steel Specimen with CFRP Overlay Elements Bonded Over the Fatigue Vulnerable Welds	12
Figure 3-2.	CFRP Overlay Elements	15
Figure 3-3.	CFRP-Stiffened Specimen Positioned in Instron Test Frame	18
Figure 3-4.	CFRP Shape Variations Modeled in Finite Element Analyses	22
Figure 3-5.	Comparison of Deflections of CFRP-Stiffened Specimens and Control Specimens	24
Figure 3-6.	Maximum Deflection of CFRP-Stiffened Specimen TRI_01 (Incrementally Increased Load)	26
Figure 3-7.	Maximum Deflection of CFRP-Stiffened Specimen TRI_02 (Redesigned Overlays, Constant Load)	27
Figure 3-8.	Comparison of Model and Experimental Deflections for CFRP-Stiffened Specimen	30
Figure 3-9.	Comparison of Stress Data for Finite Element Models with CFRP Overlay Shape Varied	31
Figure 4-1.	Schematic of Three Point Bending Fixture with CFRP-Stiffened Specimen	40
Figure 4-2.	S-N Diagrams of Fatigue Test Results for Experimental and Control Specimens	42
Figure 4-3.	Shear Stress for Varied Bond Thickness from Finite Element Models	45
Figure 4-4.	Close-Up View of Leading Edge of a Debonded CFRP Overlay Element	46
Figure 4-5.	Dynamic Stiffness of CFRP-Stiffened Steel Specimens	48
Figure A-1.	S-N Data for Specimen TRI_01	59
Figure A-2.	Dynamic Stiffness Data for Specimen TRI_01	59
Figure A-3.	S-N Data for Specimen TRI_02	60
Figure A-4.	Dynamic Stiffness Data for Specimen TRI_02	60
Figure A-5.	S-N Data for Specimen TRI_04	61
Figure A-6.	Dynamic Stiffness Data for Specimen TRI_04	61
Figure A-7.	S-N Data for Specimen TRI_05	62
Figure A-8.	Dynamic Stiffness Data for Specimen TRI_05	62
Figure A-9.	S-N Data for Specimen TRI_06	63
Figure A-10.	Dynamic Stiffness Data for Specimen TRI_06	63
Figure B-1.	Mold Base with Gasket Material	67
Figure B-2.	Mold Base with Sidewall	67
Figure B-3.	Mold Base with Sidewall and Ends	68

Figure B-4.	Properly Positioned Mold Pieces	68
Figure B-5.	Assembled and Fully Tightened Mold Body	69
Figure B-6.	View of Mold Body Cavity	70
Figure B-7.	Placement of 6 in. Carbon Fiber Base Plies	71
Figure B-8.	Placement of Carbon Fiber and Resin Film Rolls	72
Figure B-9.	Placement of Carbon Fiber Plies	73
Figure B-10.	Placement of Boron Fiber Ply	73
Figure B-11.	Placement of Resin Film Strip	74
Figure B-12.	Mold Body and Former Block	75
Figure B-13.	Former Block Fully Positioned in Mold Body	75
Figure B-14.	Press Plate Fully Positioned in Mold Body	76
Figure B-15.	Fully Assembled Mold	77
Figure B-16.	Assembled Mold Positioned in Heat Press	78
Figure B-17.	Assembled Mold Subjected to Load and Temperature in Heat Press	79
Figure B-18.	Mold Ready to be Taken Apart	80
Figure B-19.	Mold with Threaded Fasteners Removed	80
Figure B-20.	Mold with One Sidewall Released	81
Figure B-21.	Remaining Mold Pieces with Sidewalls and Press Plate Removed	81
Figure B-22.	Chisel Driven Between Mold Base and Former Block	82
Figure B-23.	Release of Former Block from Mold Base	83
Figure B-24.	Chisel Driven Between Mold Base and CFRP Overlay Element	84
Figure B-25.	CFRP Overlay Element Removed from Mold	85
Figure B-26.	Post-processing of CFRP Overlay Element Sides	86
Figure B-27.	Post-processing of CFRP Overlay Element Ends	86
Figure B-28.	Post-processed CFRP Overlay Element and Removed Material	87
Figure C-1.	Schematic of Tensile Test Specimens	93
Figure C-2.	Stress vs. Strain Curves for Tensile Specimens (Max. Load of 500 lb.)	95

LIST OF TABLES

Table 4-1.	Fatigue Testing Results for CFRP-Stiffened Specimens and Control Specimens	38
Table C-1.	Test Specimen Dimensions	94

LIST OF SYMBOLS

<u>Symbol</u>	<u>Description</u>	<u>Units (SI, USImp.)</u>
a	Tab Length	[mm], [in.]
d	Depth	[mm], [in.]
E	Modulus of Elasticity	[MPa], [ksi]
K_{dyn}	Dynamic Stiffness	[kN/mm], [kip/in.]
L	Specimen Length	[mm], [in.]
N	Fatigue Loading Cycles	
ΔP	Change in Applied Load	[kN], [kip]
t	Thickness	[mm], [in.]
Δy	Change in Deflection	[mm], [in.]
x	Longitudinal Distance	[mm], [in.]
ε	Strain	[mm/mm], [in./in.]
$\Delta\sigma$	Stress Range	[MPa], [ksi]
σ	Stress	[MPa], [ksi]
τ	Shear Stress	[MPa], [ksi]

LIST OF ACRONYMS

<u>Acronym</u>	<u>Description</u>
AASHTO	American Association of State Highway and Transportation Officials
AISC	American Institute of Steel Construction
CFRP	Carbon Fiber Reinforced Polymer
FEA	Finite Element Analysis
FRP	Fiber Reinforced Polymer
LRFD	Load and Resistance Factor Design
MVCCT	Modified Virtual Crack Closure Technique

CHAPTER 1 - INTRODUCTION

1.1 RESEARCH OBJECTIVES

The use of CFRP materials in structural engineering has only become a reality in recent years. The majority of the applications of these composites to structures have been with relation to the shoring up and strengthening of concrete structures (see the proprietary literature of companies such as Sika Corporation and others for more information about the use of CFRP for concrete). Only minimal effort has been employed investigating CFRP materials for steel structures, though the potential in this area is excellent, especially with respect to mitigation and enhancement of fatigue-vulnerable steel details. The overall objective of research presented in this thesis was to prove the viability of CFRP materials in a fatigue enhancement application.

To accomplish this primary objective the research progressed through several complimentary objectives. First, a CFRP material that with the desired characteristics had to be developed. This included the design of the composite by choosing raw materials from which it was to be constructed as well as choosing and perfecting the method of manufacture for the composite. Accomplishing this first goal proved to be a significant undertaking.

Next, the CFRP material (henceforth referred to as the CFRP overlay) had to be tested while applied to a steel detail. This required the selection of an appropriately fatigue-vulnerable steel specimen and a bonding agent to facilitate load sharing between the CFRP overlays and the steel. Thus, the second complimentary objective was to show through fatigue testing that the CFRP overlays could provide a significant improvement in fatigue life of the steel detail.

Details of the complimentary objectives will be presented further in Chapters 3 and 4.

1.2 DIVISION OF RESEARCH

The tasks required to accomplish the research presented in this thesis fell naturally into two distinct categories: CFRP overlay development and fatigue

enhancement testing. A chart showing the general procedure followed during this project is presented in Figure 1-1. Discussion items such as experimental set-up, testing procedures, testing goals, and data analysis differed significantly between these two categories of effort, so much so that two journal articles were written on this research, one relating to each category. Thus, it was deemed just as appropriate to present the data and results of the project in two separate discussions within this thesis as well.

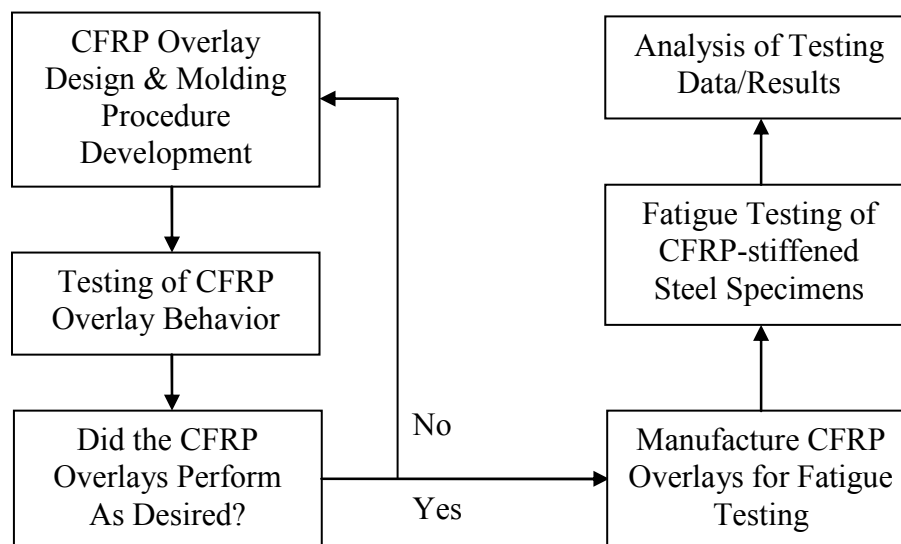


Figure 1-1. General Research Procedure

Background information for both phases of the research is presented in Chapter 2. Chapter 3 is devoted entirely to the development of the CFRP overlays, with the experimental setup, and discussion of results pertaining to the composite overlay development included. Chapter 4 is devoted entirely to the investigation of the fatigue enhancement capabilities of the CFRP overlays through cyclic testing. Experimental setup, and discussion of results pertaining to this testing are discussed therein. Overall conclusions and recommendations are presented in chapter 5.

A full compliment of plots describing the data recorded while testing the specimens in this research project are provided in Appendix A, and Appendix B provides the steps followed to manufacture the CFRP overlays that were used in the testing. Information on bonding of the CFRP overlays is also included in Appendix B. Appendix C contains supplemental information required for the efforts of this research comprising tensile testing of the CFRP material per ASTM D3039.

CHAPTER 2 – BACKGROUND INFORMATION & LITERATURE REVIEW

2.1 GENERAL BACKGROUND INFORMATION

In recent years, several methods have been developed to enhance fatigue critical details in steel bridges and other steel structures. The simplest of these methods can be employed during the design phase of a project by ensuring that a structural detail will not be subjected to states of stress that might cause fatigue crack initiation. For example, a designer can ensure that no section of the structure is subjected to a state of complete constraint (tri-axial stress) (Barsom and Rolfe 1999). The importance and applicability of this methodology has been reinforced historically in many instances, including the multiple failures in steel connections that took place during the Northridge Earthquake of 1994. The AISC Steel Construction Manual (2005) specifically addresses this method as a paramount consideration for designers of steel structures.

However, if a structure is already constructed and it is undesirable or cost prohibitive to replace existing fatigue critical details, then alternative methods must be employed to enhance the fatigue life. One such method available for welded connections is to utilize an ultrasonic impact device, and create a region of compressive residual stress at the toe of the weld (Statnikov 2004). Ultrasonic impact treatment (UIT) can effectively prevent crack formation at fatigue-critical welds by significantly decreasing the magnitude of tensile stresses at the weld toe due to cyclic loading, which virtually eliminates crack formation and greatly increases the fatigue life of the detail (Statnikov 2005). Other methods of introducing compressive residual stresses, such as shot peening, air hammer peening, and laser peening can be used in a similar manner to

improve the fatigue performance of welded structural details. Alternatively, it is proposed that stresses at some welds can be reduced by application of a stiff overlay material, such as CFRP. This is the approach to fatigue enhancement discussed in this paper.

2.2 CFRP MATERIALS

Laminar CFRP materials are often manufactured by stacking layers (plies) of graphite fibers and a bonding material (polymer matrix), and then subjecting the stack to heat and pressure. The heat activates the matrix material, causing it to flow and completely surround the fibers. Application of pressure reduces the amount of air voids throughout the depth of the composite, forcing the air out with any excess matrix material. The relative volume fractions of the voids, fibers, and matrix material in the finished composite, known as consolidation, are used to categorize the quality of the composite. Composites with high levels of consolidation (fiber volume fractions greater than 60%, matrix volume fractions lower than 40%, and negligible void volume fractions) have higher strength and stiffness characteristics than poorly-consolidated composites, and are more resistant to crack propagation and internal delamination (Mallick 1993). A common matrix material for CFRP in engineering applications is resin epoxy. When activated through heat application, resin epoxy undergoes a chemical reaction in which the polymer molecules of the resin develop cross-linked bonds and form a solid structure. This type of resin is known as thermo-set, which implies that after the cross-linked structure is formed, the resin will no longer flow even

if re-heated to the original activation temperature (although at elevated temperatures the structural rigidity of the resin epoxy does decrease).

2.3 LITERARY REVIEW OF PREVIOUS INVESTIGATIONS UTILIZING CFRP MATERIALS FOR FATIGUE ENHANCEMENT OF STRUCTURAL STEEL

Several previous studies have focused on application of FRP to improve fatigue performance of connection details in steel bridges (Bassetti et al. 2000). However, the challenge for practical application has been to provide a strong and durable bond between the steel and composite such that load sharing can be accomplished. Internal and external delaminations have been common problems for investigations examining the use of composite materials applied to steel structural members (Colombi et al 2003). Often the bond material is not capable of resisting shear stresses high enough to continually provide load sharing between the bonded materials for a significant number of load cycles. Additionally, once a crack begins to form in the bond, it has tended to propagate quickly due to the brittle behavior of most bond materials at standard testing temperatures (Hertzberg 1996).

Reinforcement of connections in steel structural members with strips of CFRP material has been investigated by Bassetti et al (2000). For their investigations, holes were drilled at the center of steel plates, and then crack-like flaws were created extending out from the hole by the method of electroerosion. The plates were then reinforced on either side with pultruded CFRP strips 50 mm (2 in.) in width that contained unidirectional carbon fibers. These strips were bonded to the steel plates

with a viscous two-part epoxy. The goals of the studies were to show the effectiveness of the application of CFRP materials for fatigue life enhancement, and to show the further effectiveness of the CFRP materials if they are prestressed prior to application. The prestressing of the composites prior to bonding causes a region of compressive stress in the final (cured) specimen, which has the effect of lowering the apparent stress range to which the flaw is subjected. Bassetti et al. expressed the view that use of unusually thick CFRP materials was impractical. The unstressed and prestressed specimens were subjected to fatigue testing at a stress range of 80 MPa (116 psi) and a stress ratio

$R = 0.4$. Crack growth was measured for the specimens specified previously and for control specimens with respect to the number of applied load cycles. It was determined that the application of the unstressed CFRP strips increased the fatigue life of the specimens by a factor of three, and the prestressed CFRP strips increased the fatigue life of the specimens by up to a factor of sixteen. The CFRP strips were also fitted to a 91-year old bridge of riveted construction to further prove the viability of CFRP materials as a reinforcement of steel structures. It was noted, however, that while the CFRP materials did cause an enhancement of the fatigue life of the specimens tested, the overall effectiveness of the composites was thought to be hampered by debonding from the steel as crack growth persisted. This debonding lessened the effect of the CFRP strips, which allowed acceleration of crack growth, and led to further debonding. It was determined that the debonding was occurring at the interface between the steel and the bond material, and generally not between the bond material and the CFRP

strips. Additionally, it was observed that the debond was elliptical in shape with an aspect ratio of 1/5.

It became clear that understanding the mechanisms that affect debonding of composites was very important for design of specimens utilizing CFRP material as an enhancement technique. Colombi et al (2003) performed several investigations of the specimens tested by Bassetti et al (2000) with goal of using finite element models to evaluate the effects of composite pretension, composite stiffness, composite thickness, and bond thickness on the stress intensity factor, K , of the crack-like flaw in the specimens; and to evaluate the effects of composite pretension, bond thickness, and debond shape on the strain energy release rate over the flaw surface. The finite element models used for the investigations were created using the ABAQUS FEA software, and were based on Mindlin Plate Theory (Colombi 2003), which assumes a linear displacement field over defined strata (layers or plates). To characterize the debonding of the CFRP strips, the strain energy release rate, G , was calculated from finite element models using the modified virtual crack closure technique (MVCCT). It was determined that thinner bond thickness, absence of pretension, and smaller elliptical aspect ratio allowed for higher strain energy release rates, which equated to faster crack growth in the specimens (Colombi et al 2003). Additionally, it was determined that the effectiveness of the composites for the fatigue enhancement of the specimens (measured by the calculated K value) increased as the CFRP strip thickness was increased, but decreased as the bond thickness was increased. Use of CFRP materials with higher stiffness and prestressing of the CFRP strips increased their effectiveness as well (Colombi 2003).

It is recognized that FRP composites are generally most efficient when fibers are placed to the greatest extent possible in tension. With this in mind, an extensive multi-part study was conducted to investigate the effectiveness of CFRP materials as a fatigue life enhancement mechanism by Nozaka et al (2005). Strips made from several types of CFRP materials (Carbodur and Tyfo UC) were bonded to steel coverplates that were then bolted to the tension flange of a W14x68 beam made from A572 Grade 50 steel which was loaded in four point bending. A thin cut was made in the beam flange, and the cut was extended into the beam web where it connected with a large hole. These stress concentrators were intended to create a region of higher tensile stresses in the beam flange at the middle of the span. Tensile stress and stiffness of the CFRP materials were determined by testing in accordance with ASTM D3039. The variables in the study apart from the CFRP materials were the type of adhesive used to bond the strips, and the configuration of the coverplates. Five different adhesives were investigated including Sikadur 330, Sikadur 30, PLUS 25, DP-460 NS, and Tyfo TC (Nozaka et al 2005). Five geometric configurations were also investigated with variations in the gap between the steel coverplates as well as the extent of the CFRP strip area that was bonded. Twenty-seven specimens were tested in the study, and based on the results, Tyfo UC CFRP bonded with the DP-460 NS adhesive was recommended as the most advantageous of the tested combinations (Nozaka et al, 2005). It was determined that leaving a region of the CFRP strips unbonded on either side of the cut in the beam produced the highest tensile strain in the composites, and increasing the number of layers (plies) in the CFRP strips increased the maximum

moment at failure of the specimens. Experimental results of the study were supported by data from finite element models created using ABAQUS FEA software.

Thus, from an examination of previous research, several techniques were revealed that could aid in optimizing the effectiveness of CFRP materials for fatigue enhancement of steel details. First, the bond between the steel and composite must be comprised of a material that is durable, strong, and able to withstand significant levels of shear stress. Second, the thickness of the bond material greatly affected the extent of load sharing between the steel and composite, so further testing should include investigation of multiple bond thicknesses. Third, an increased number of plies in the composite (maximized thickness) when used as an overlay on a fatigue-vulnerable detail on the flange of a steel girder increased the maximum moment the detail could withstand, and thus decreased the stress demand at the design moment. Next, use of finite element modeling as predictive aid to the testing of these specimens helped to focus experimental work and pare down the number of variables associated with the use and testing of composite materials. Finally, while it was not included in this investigation, prestressing of CFRP materials was shown to be effective in previous investigations. It should also be noted that previous studies focused on using CFRP strips to lengthen the propagation fatigue lives of already-cracked specimens. The study described in this paper focused on increasing the crack initiation fatigue life of uncracked specimens.

CHAPTER 3 – CFRP OVERLAY DEVELOPMENT

3.1. OBJECTIVE

The objective of the CFRP overlay element development was to design and manufacture a CFRP overlay with stiffness and strength characteristics such that the overlay would increase the overall stiffness of a fatigue-critical connection when fully bonded, providing an alternate load path, thereby reducing the peak stress at the detail. A secondary objective was to ensure that the CFRP overlay element was robust enough to withstand a significant number of fatigue cycles without internal or bond degradation.

3.2 EXPERIMENTAL SETUP

A retrofit that was formerly common practice in bridge design was to attach steel coverplates to the flanges of steel bridge girders in regions of high moment demand. From a connection standpoint, welding of the coverplates provides the most efficient means of ensuring shear and load transfer while minimizing shear lag. However, from a fatigue standpoint, the use of welds creates innumerable sites from which cracks can initiate and propagate. One such detail has proven to be so prone to development of fatigue cracks that the AASHTO LRFD Bridge Design Specifications (2007) categorize it with the worst fatigue rating possible, denoted as Category E'. Since the aim of this research was to prove the viability of CFRP doubler elements in the enhancement of fatigue life, the aforementioned fatigue-vulnerable detail was

chosen as the specimen to which the CFRP double elements would be applied. This was advantageous as the detail itself was not overly complex in terms of geometry.

3.2.1 STEEL SPECIMENS

The steel specimens to which CFRP doublers were later bonded were comprised of two 25.4 mm (1.00 in.) thick plates welded together with a 7.94 mm (5/16 in.) fillet weld. All steel specimens were A36 grade steel. One of the two plates was wider and longer than the other, with the larger representing a bottom flange of a steel girder, and the smaller representing a coverplate. Dimensions of the welded coverplate were such that the detail was categorized as an AASHTO (2007) Category E' fatigue detail. Figure 3-1 shows the specimen with the CFRP overlay elements affixed (two per specimen). Dimensions of the steel specimens were chosen to balance the affects of shear lag and stress distribution considerations according to St. Venant's Principle (Vilhauer 2007).

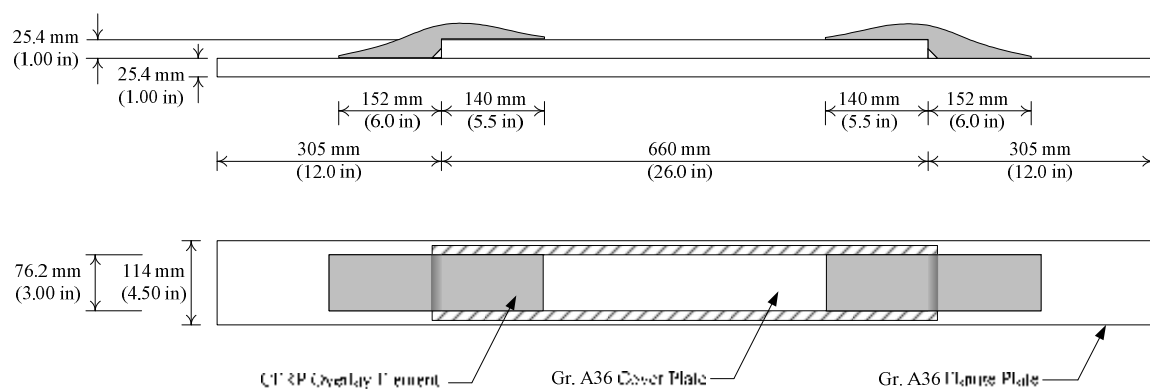


Figure 3-1. Steel Specimen with CFRP Overlay Elements Bonded Over the Fatigue-Vulnerable Welds

3.2.2 CFRP OVERLAY DEVELOPMENT

Initial focus of the CFRP overlay development was to produce overlay elements with sufficient thickness to have a significant stiffening effect on fatigue details within the steel specimen. The thickness of the overlays when bonded to the steel served to increase the bending moment of inertia of the specimen around the fatigue-critical welds. This was achieved with very little increase in overall specimen weight, due to the low self weight of the CFRP materials used. The intent of the increased moment of inertia was to cause the specimen to have increased stiffness, smaller deflections, and a lower stress demand in the area surrounding the welds. To achieve increased thickness in the CFRP doublers, a greater number of plies were used in comparison to conventional CFRP composites. In general, the greater the number of plies that are used, the more difficult it becomes to achieve good consolidation of the composite using standard vacuum-bag methods to apply pressure during the molding process.

The curvilinear shape and overall dimensions of the CFRP overlays were chosen to provide large bond areas while also providing efficient load transfer from the steel to the composite material over the weld at the end of the coverplate. It was considered paramount to have the graphite fibers laid in continuous fashion from the base steel plate to the coverplate, thus rolls of graphite fabric were placed at the change in thickness between the base plate and cover plate to keep the continuous layers from drifting too far from their planar orientation. The rolls were not included in the ply counts, and initially were not considered to add to the overall composite strength.

After several preliminary attempts with plies numbering as high as two hundred per CFRP overlay, a formula was chosen using 36 plies of bi-directional woven carbon-fiber material (Cytec Fiberite 976 series fabric pre-impregnated with cyanamide-123 resin) and a vacuum pressure just slightly above atmospheric pressure (approx. 1.1 bar) combined with an activation temperature of 121 °C (250 °F) provided by a laboratory oven. At this combination of heat and temperature, the resin was fully cross-linked in six to eight hours. The consolidation of composites produced using this methodology was poor, with a significant amount of air voids remaining in the material. Additionally, the curvature of the doubler elements was variable, but the thickness at the step remained approximately uniform (see Figure 3-2a). The poor consolidation was initially deemed acceptable in an effort to maximize the dimensional thickness of the composite, which was on average 25.4 mm (1 in.) thick at the step. To eliminate edge effects on the composite arising from the mold surfaces, the CFRP material was initially molded with a width of 101.6 mm (4 in.). After the molding process was completed, the CFRP was allowed to cool, removed from the mold, and cut down to a width of 76.2 mm (3 in.) to match the width of the detail on the steel specimen. Figure 3-2a shows the initial doubler lay-up (stack of plies) after the vacuum bag molding process was completed.

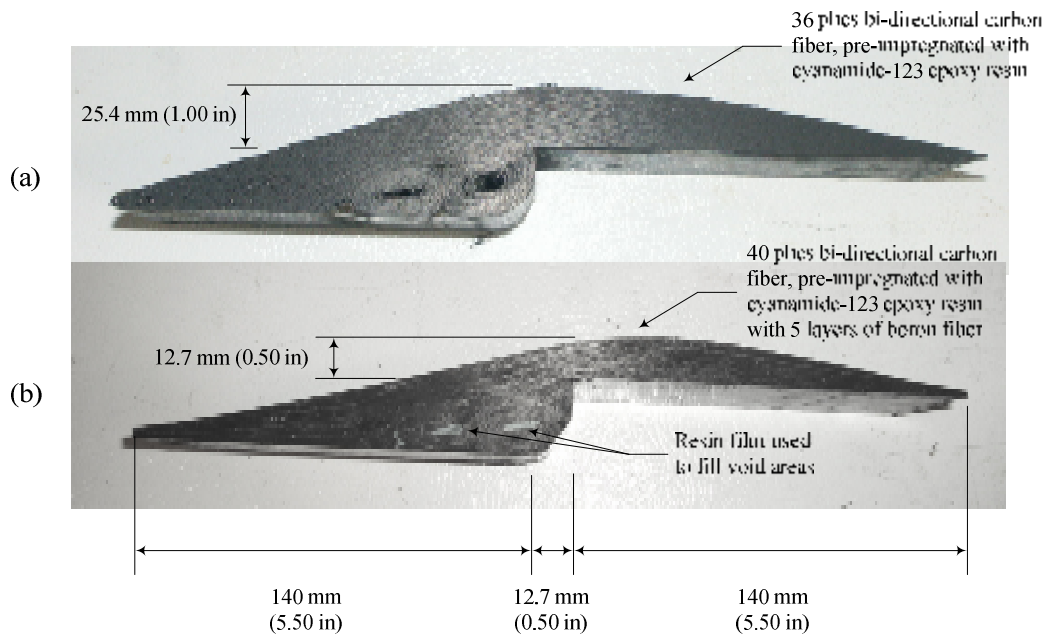


**Figure 3-2. CFRP Overlay Elements: (a) CFRP Overlay with Low Consolidation Level,
 (b) Redesigned CFRP Overlay with High Consolidation Level**

Initial testing of the doubler-reinforced steel specimens indicated that the CFRP doubler elements should be redesigned with a focus on consolidation instead of dimensional thickness. To achieve optimal consolidation, a heat press was chosen as an alternate method to apply pressure and heat during the molding process. A new mold was machined from thick aluminum plate that could withstand very high applied pressure. After several iterations, the number of carbon fiber plies was increased to 40, five boron-fiber layers were added, and resin film was incorporated into the lay-up. Boron-fiber layers prevented the carbon-fiber fabric layers from migrating too far out of plane during the heat-press mold process. Resin film supplied additional resin in areas where voids could not be eliminated even with increased mold pressure. Figure 3-2b shows the redesigned doubler lay-up after the heat press molding process. Details of the molding process are provided in Appendix B.

The heat press molding method allowed the CFRP to be molded with an applied force of 62.3 kN (14 kip) and a temperature of 177 °C (350 °F). The applied force on the mold provided a pressure of 18.1 bar, or 1.81 Mpa (263 psi), a significant increase from the pressure supplied by the vacuum bag technique used initially. Using the heat press method, the resin was fully cross-linked in three to four hours. To eliminate edge effects between the plies and the mold surfaces, the CFRP was molded to a width of 96.5 mm (3.80 in.). After the mold had cooled and the composite was removed, it was cut down to a width of 76.2 mm (3.00 in.). Additionally, the ends of the doubler were squared off such that the thickness at the end was 2.00 mm (0.10 in.) to eliminate flaws that were highly susceptible to initiation of internal delamination of the composite layers. The CFRP overlay elements produced using this method were uniform in shape, and had high levels of consolidation, but the thickness at the step was reduced to an average of 12.7 mm (0.50 in.) as shown in Figure 3-2b.

The CFRP overlay elements were bonded to the steel specimens using Hysol (Loctite 9412), a commercially-available high-grade resin epoxy. The steel surfaces were prepared using a standard hand grinder and degreased using isopropyl alcohol. The composite overlay surfaces were roughened using 100-grit sandpaper, and were also degreased using isopropyl alcohol. The bond between the CFRP overlay and the steel substrate was cured at room temperature for a minimum of 48 hours before any load was applied.

3.2.3 FATIGUE TESTING EXPERIMENTAL SETUP

The CFRP-stiffened steel specimens were subjected to fatigue loading in a three-point bend test fixture in an Instron model 1334 closed-loop servohydraulic test frame with a static load rating of ± 489 kN (110 kip) and a fatigue load rating of ± 240 kN (55 kip). The test frame was actuated by a 8800D computer control system, and cyclic fatigue loads for all specimens were applied such that the minimum load was one-tenth the maximum load ($R = P_{\min} / P_{\max} = 0.1$). The loading was cycled at rates of 1.5 to 2 Hz. Figure 3-3 shows a photograph of a CFRP-stiffened specimen positioned on the test fixture in the Instron test frame.

The computer controller for the Instron test frame monitored maximum and minimum loads, maximum and minimum deflections, and average loads and deflection for each loading cycle. The data was saved to a spreadsheet file every 50th cycle, while the trend of data for the last ten cycles was displayed on the controller screen.

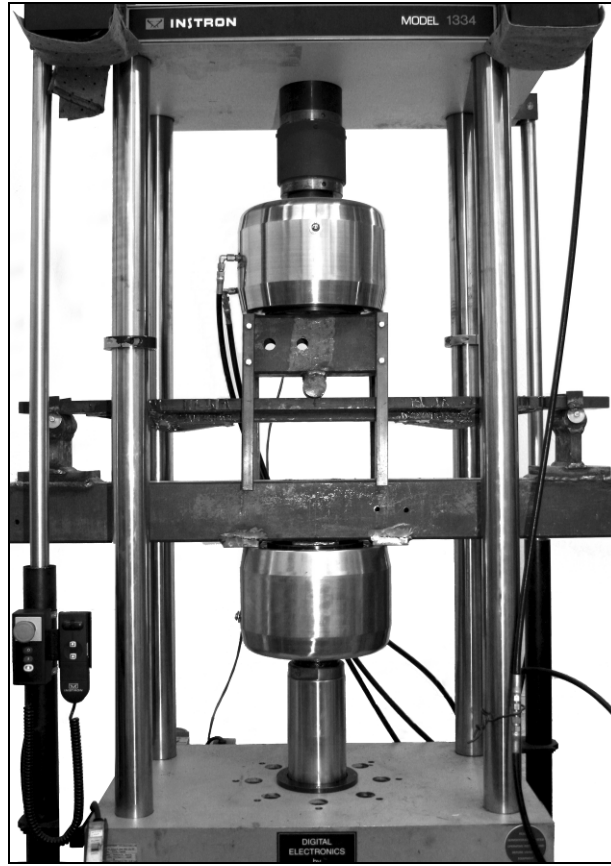


Figure 3-3. CFRP-Stiffened Specimen Positioned in Instron Test Frame

For the initial test (specimen TRI_01), the durability of the CFRP material and the steel-to-composite bond were unknown, so the initial loading was chosen such that the theoretical stress range at the weld toe for the control specimen was 58.6 Mpa (8.50 ksi), which equated to an applied load range of 7.00 kN (1.54 kip) at the centerline of the steel specimen. This was a relatively low stress range, and for a category E' detail the AASHTO LRFD Bridge Design Specification (2007) estimates a design life at this stress range of approximately 700,000 cycles. The CFRP-stiffened specimen TRI_01 was tested at 2 Hz until it reached 1.1M cycles, at which point the bond between the steel and the CFRP overlays were deemed to have sufficient strength at that stress

range. No fatigue crack formation was observed in the steel, and no degradation was observed in the CFRP material or the bond between the steel and composite. The load range was then increased incrementally, in a step-wise function from 58.6 MPa (8.50 ksi) to 86.2 MPa (12.5 ksi) to 100 MPa (14.5 ksi) to 110 MPa (16.0 ksi) and to 138 MPa (20.0 ksi), to determine the maximum stress range that the CFRP overlay could withstand under cyclic loading. This step-wise loading was also chosen for this initial fatigue test to determine the mode of failure of the CFRP-stiffened specimen to help guide further development. The ratio of minimum to maximum loads in all cases remained at $R = 0.1$.

After the initial test, a control specimen that had received no CFRP treatment was cycled briefly at a stress range of 58.6 MPa (8.50 ksi) and 110 MPa (16 ksi), for the purpose of recording deflections across its entire length using dial gages. These deflections were later compared with deflections measured for the stiffened specimen within the 58.6 MPa (8.50 ksi) and 110 MPa (16 ksi) portions of that test, and are included in the discussion of results.

A second fatigue test was performed on a steel specimen outfitted with the redesigned, well-consolidated CFRP overlays (specimen TRI_02). This second fatigue test was performed at a stress range of 138 MPa (20.0 ksi) and a similar loading rate as the first. The test was performed until both CFRP elements debonded and the steel specimen failed due to complete propagation of a fatigue crack. Deflections were compared directly before and after it was observed that the CFRP overlay had debonded using the deflection readings from the Instron test frame LVDT which was located at the centerline of the specimen.

Testing was also performed on unstiffened steel specimens to comprise a control group (Vilhauer 2007). Three unstiffened steel specimens were tested; two were tested at a stress range of 138 MPa (20.0 ksi) and one at a stress range of 58.6 MPa (8.50 ksi). These control specimens were cycled using the same equipment as described above, and the ratio of minimum to maximum load was also set at $R = 0.1$.

3.2.4 FINITE ELEMENT MODELING EXPERIMENTAL SETUP

Due to the uniqueness and complexity of the composite overlays, finite element models were created with the goals of predicting the behavior of the stiffened steel specimens and determining the effects of several key parameters for the CFRP overlays. The parameters investigated were: profile shape of the overlays, size of the bonded surfaces between the CFRP overlays and the steel specimen, thickness of the bond between the two materials, and stiffness of the composites. The material properties assigned to the models were consistent with A36 steel and the results of tensile testing performed on the CFRP material in accordance with ASTM D3039. Detailed information on the tensile testing is given in Appendix C.

2-D and 3-D finite element models of the control and CFRP-stiffened steel specimens were constructed using the commercially available ABAQUS finite element analysis software (version 6.7). The 2-D models were comprised of a 25.4 mm (1.00 in.) wide portion of the specimen while the 3-D models were comprised of the full width of the specimen. In both cases, the models of the base steel specimen, weld, and composite were created and meshed separately, then assembled using interaction

surfaces to define the type of interaction between the meshed bodies (i.e. rigid connection, hard contact, etc.). Additionally, the meshes around the location of the weld were refined such that element sizes were decreased to account for stresses and strains that were expected to be vary significantly in these regions. Welds were modeled as having a triangular cross-section, with the two legs being of equal length.

The boundary conditions for the models were created to match the simple supports of the physical test specimens. These were defined in the model by restricting only vertical translations at both of the support locations and also restricting longitudinal translations at one end of the model. Translations were restricted in the transverse direction to eliminate model instability. These boundary conditions effectively modeled the three-point bending apparatus used in the physical tests.

Loads were applied to the models at the centerline of the meshed geometry, and the magnitude of the loads were such that they matched the theoretical stress ranges at the weld toe of the control specimen as chosen for the physical specimen testing. For the 3-D models, the applied load was a pressure load over a thin area at the center of the model. For the 2-D models, the applied load was a point load. Loads applied to the 2-D model were scaled down since these models were based on a thickness of 25.4 mm (1.0 in.). Loads applied to the 3-D model were numerically identical to the loads applied to the physical specimens. In all models, nominal stresses were matched to the nominal stresses in the physical control specimens at the toe of the weld.

One distinct advantage to the use of finite element models to support an experimental study is that many variables and parameters can be investigated with a minimal time investment. This effort can illuminate potentially crucial parameters in

the testing program that may not have initially been considered, and can give an indication of variables or parameters that may not have as significant an effect as was hypothesized. In several models, geometry of the composite overlay was changed to determine if this parameter had any effect on the overall stiffness of the model. Comparisons were made between rectangular and curvilinear shapes, as shown in Figure 3-4. Additionally, sizes of the bonded surfaces between the CFRP element and the steel were varied such that the surfaces ran right to the weld, or stopped short of the weld leaving an unbonded gap.

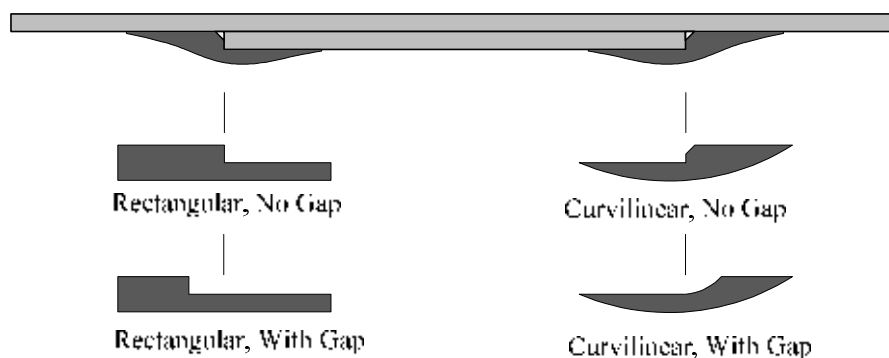


Figure 3-4. CFRP Overlay Shape Variations Modeled in Finite Element Analyses

This gap region was modeled as a parameter to investigate the assumed ineffectiveness of rolled plies near the step in the actual composite overlay elements. Another parameter that was investigated was bond thickness between the CFRP element and the steel. Two bond behavior boundaries were modeled: an extremely stiff bond was modeled using tie constraints, and an extremely pliable bond was modeled using a hard contact surface. The final parameter that was investigated was the stiffness of the

CFRP material. All results of the parametric investigations are described in the following section.

3.3. DISCUSSION OF RESULTS

Experimental testing as part of the CFRP overlay element development was performed in parallel to modeling of the specimens with finite element software. This tactic proved to be advantageous as the two forms of investigation at times corroborated each other, and at others helped to focus the other. The results of both are presented in succession in this section.

3.3.1 EXPERIMENTAL TEST RESULTS

Data from the initial fatigue test (specimen TRI_01) showed that despite poor CFRP consolidation, the initial overlays provided a significant increase in specimen stiffness when compared with control specimen stiffness. Figure 3-5 shows the deflections recorded with dial gages for the control and CFRP-enhanced specimen TRI_01 during the 58.6 MPa (8.50 ksi) and 110 MPa (16 ksi) portions of the initial testing. The data taken for the control specimens is shown with the dashed curves, and the data taken for the CFRP-enhanced specimens is shown with the solid curves. At both stress ranges, the enhanced specimens exhibited smaller deflections than the control specimens, which is a direct indication that the stiffness of the enhanced specimens was increased. At the 58.6 MPa (8.50 ksi) stress range the centerline

deflections were decreased by 32.1% from 1.33 mm (0.053 in.) to 0.90 mm (0.036 in.), and at the 110 MPa (16 ksi) by 20.5% from 2.60 mm (0.102 in.) to 1.90 mm (0.081 in.).

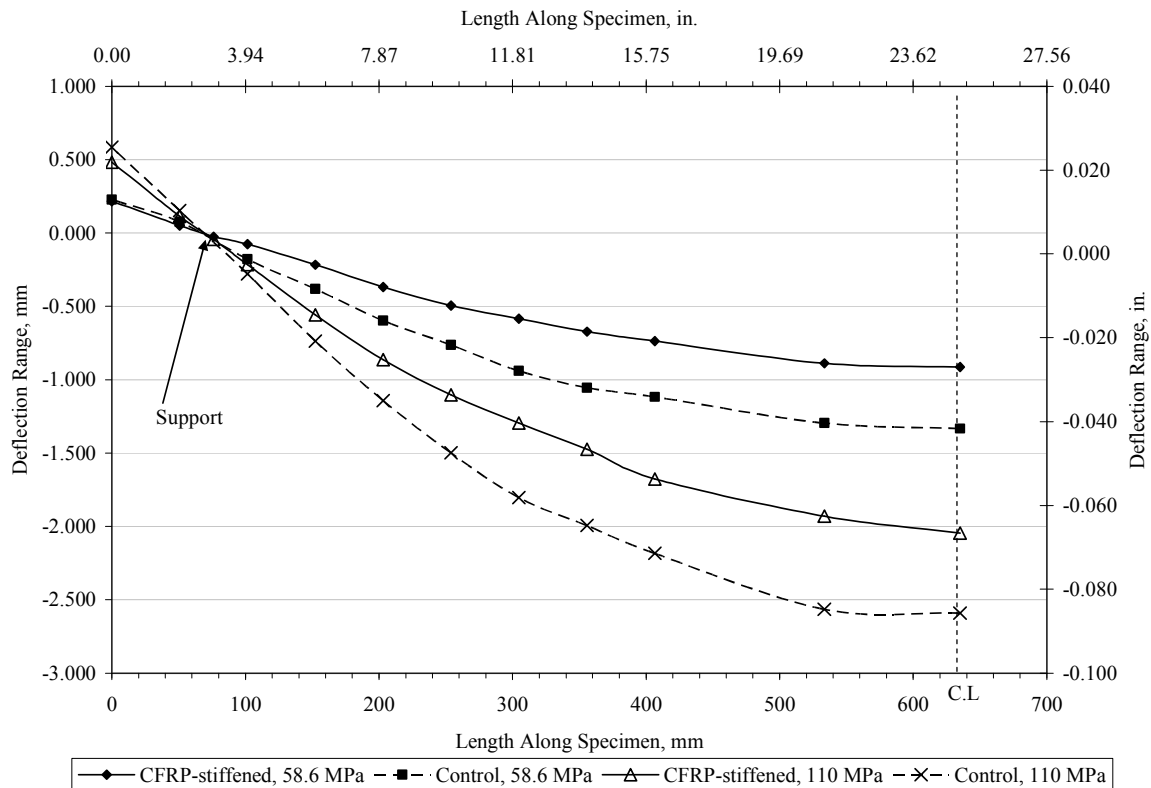


Figure 3-5. Comparison of Deflections of CFRP-Stiffened and Control Specimens

The poor consolidation of the initial version of the CFRP overlay element did have an effect on the test results. The CFRP began to undergo inter-laminar cracking at the 110 MPa (16 ksi) stress range and internal delamination occurred at the 138 MPa (20 ksi) stress range with no degradation of the bond between the composite overlay and the steel. In Figure 3-6, the regions of inter-laminar cracking and internal delamination are denoted, and it can be seen that at constant loading the maximum deflections increased steadily over the last 140,000 cycles of the test. This was an

indication that the low level of consolidation (high void volume fraction) had weakened the composite to the point that the bond resin was able to withstand higher shear stresses due to the cyclic loading than the CFRP overlay. Therefore, the CFRP overlay was redesigned, with the goal of having the bond between the composite and the steel degrade before the integrity of the composite was affected.

After the redesign of the overlay, a second fatigue test (specimen TRI_02) demonstrated that higher consolidation, in exchange for a slimmer profile, did not adversely affect the increase in specimen stiffness provided. The peak deflections (centerline) were reduced 13.8% from 3.12 mm (0.123 in.) to 2.69 mm (0.106 in.) at an applied load of 17.08 kN (3.84 kip), which corresponded to a theoretical stress at the weld toe in the control specimen of 138 MPa (20 ksi). The similar decrease in deflections for this test compared to the first CRFP overlay test, despite the reduced thickness of the redesigned overlays, are most likely due to higher consolidation of the overlay element, which increased the composite material stiffness.

As the second fatigue test progressed, the bond between the overlay elements and the steel degraded and failed with no damage to the composite material. The first overlay debonded from the steel substrate after approximately 250,000 cycles, and the second overlay debonded after approximately 895,000 cycles. Figure 3-7 shows the maximum displacement values (centerline) for the second CFRP-stiffened specimen during testing. It was surmised after inspection of the debonded composites that the first overlay debonded earlier than the second due to several void imperfections within the bond.

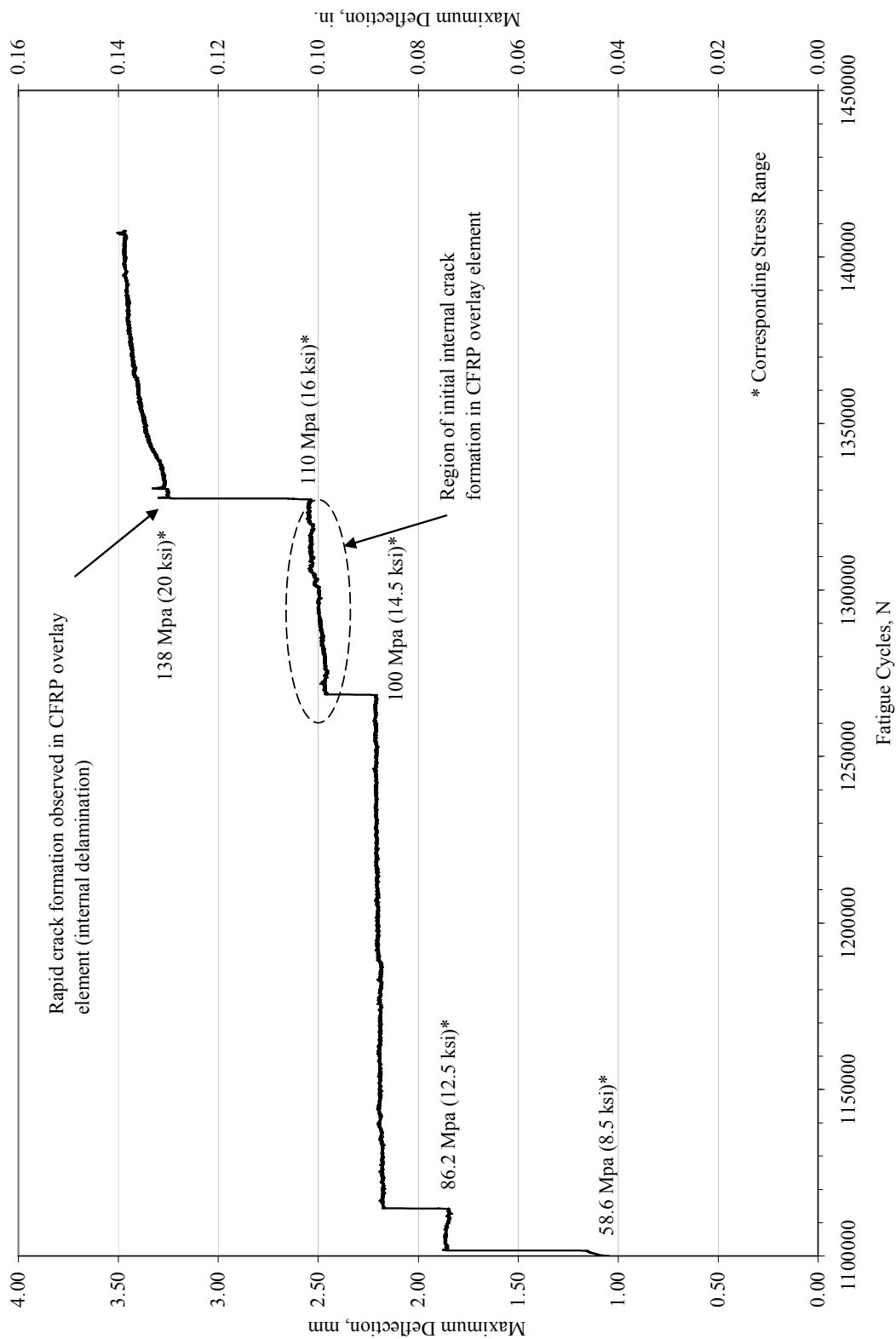


Figure 3-6. Maximum Deflection of CFRP Stiffened Specimen TRI_01(Incrementally Increased Load)

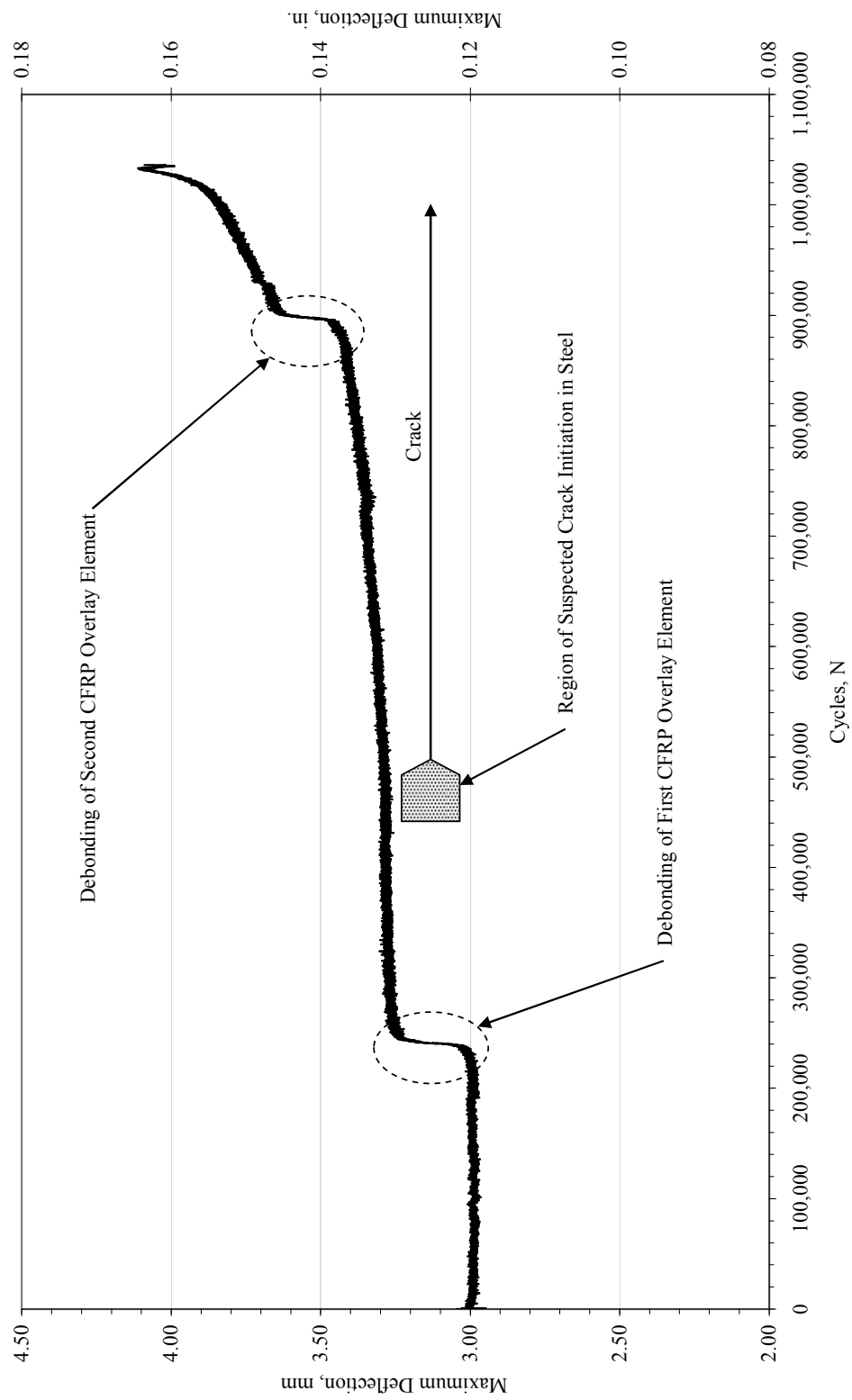


Figure 3-7. Maximum Deflection of CFRP Stiffened Specimen TRI_02(Redesigned Overlays, Constant Load)

The two control specimens tested at a stress range of 138 MPa (20.0 ksi) demonstrated crack initiation lives of 350,000 cycles and 500,000 cycles, and the control specimen tested at a stress range of 58.6 MPa (8.50 ksi) underwent 3,850,000 cycles but did not demonstrate crack initiation (Vilhauer 2007). The CFRP-stiffened specimen TRI_01 was tested at 58.6 MPa (8.50 ksi) for 1,100,000 cycles without crack initiation or degradation of the composite or bond. This seems to indicate that the stress range of 58.6 MPa (8.50 ksi) at a load ratio of $R = 0.1$ is below the threshold required for crack initiation in these specimens, and also below the threshold required to cause debonding or degradation of the composite overlay elements.

As described previously, the CFRP-stiffened specimen TRI_02 did undergo debonding of the composites, and it is surmised that crack initiation occurred at approximately 480,000 cycles. which does not represent a significant difference from the control specimens. Cracking was not observed at either of the fatigue-vulnerable welds in the specimen until approximately 200,000 cycles after the first CFRP overlay element debonded, which is supported by the data recorded during the test (Figure 3-7). The second CFRP overlay element did not undergo debonding, even after approximately 900,000 cycles, at which point the test was stopped due to the extent to which the fatigue crack had propagated at the location of the first CFRP overlay. Taking into consideration that the control specimens tested underwent crack initiation at 350,000-500,000 cycles, adherence of the second CFRP overlay element for twice that many cycles is significant. Additionally, as was discussed previously, inspection after the test revealed a large void in the bond of the first CFRP overlay element which is suspected to have greatly reduced the integrity of that bond. It is evident that in both

of the stiffened specimens tested, application of CFRP overlay elements significantly increased the overall stiffness of the specimens as evidenced by the smaller deflections recorded.

3.3.2 FINITE ELEMENT MODEL RESULTS

Modeling of the CFRP-stiffened specimens revealed that with a significantly stiff bond (one that does not undergo large shear strains), the CFRP overlay models exhibited the capability of increasing the overall stiffness of the specimen and decreasing the stress demand at the fatigue-vulnerable welds. Figure 3-8 shows a comparison of deflections between one of the models and experimental data for the first CFRP-stiffened specimen tested. The stiffening behavior of the composite overlay elements is shown by the difference in deflection between the control and stiffened specimen data sets. The difference in deflection at the centerline predicted by the finite element models is identical to that recorded during testing (0.55 mm, 0.02 in.). Thus, while the deflection data from the finite element models shown in Figure 3-8 does not align exactly with the experimental data, the decrease in deflection due to the application of the CFRP overlay elements was predicted with a high degree of accuracy.

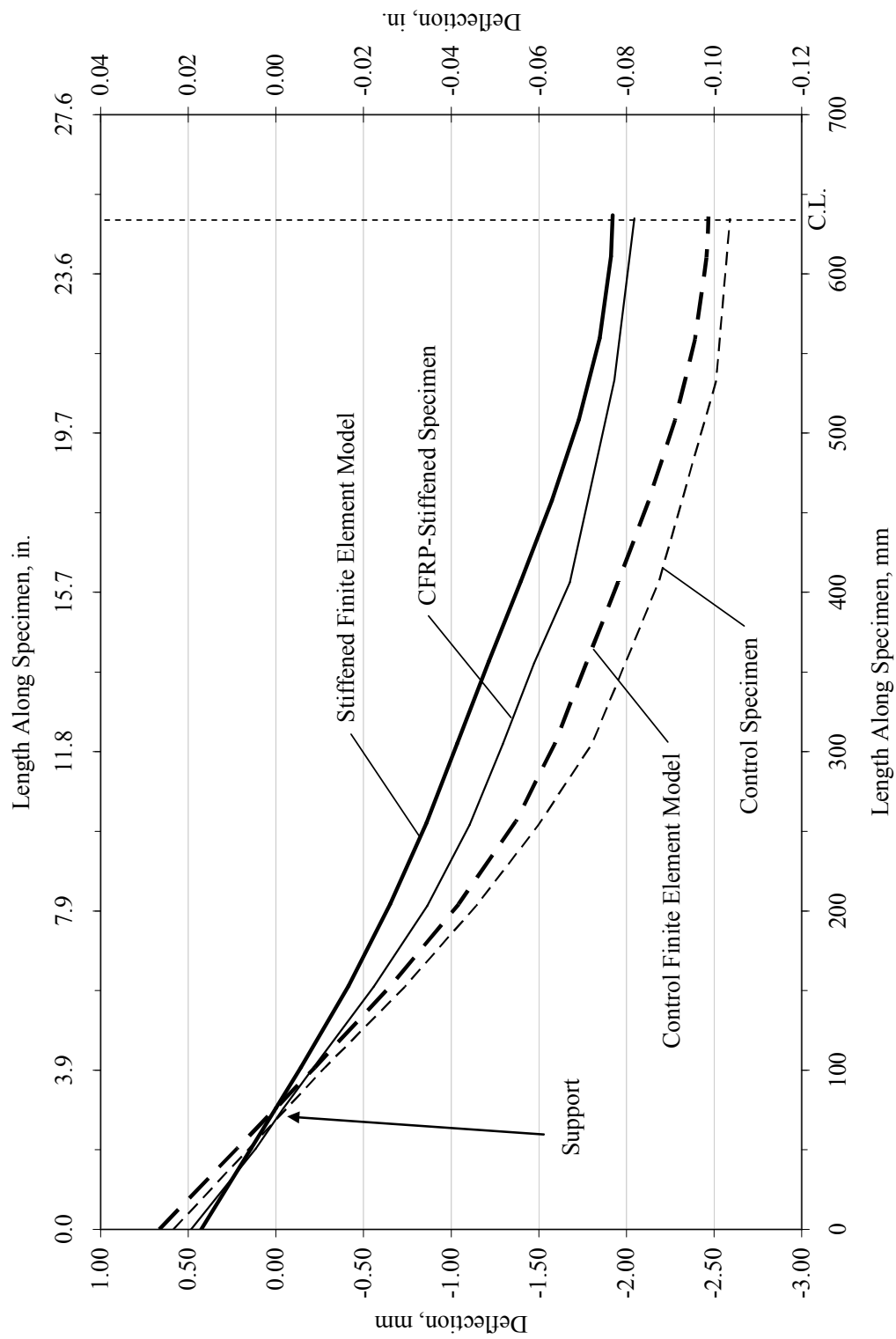


Figure 3-8. Comparison of Model and Experimental Deflections for CFRP-Stiffened Specimen

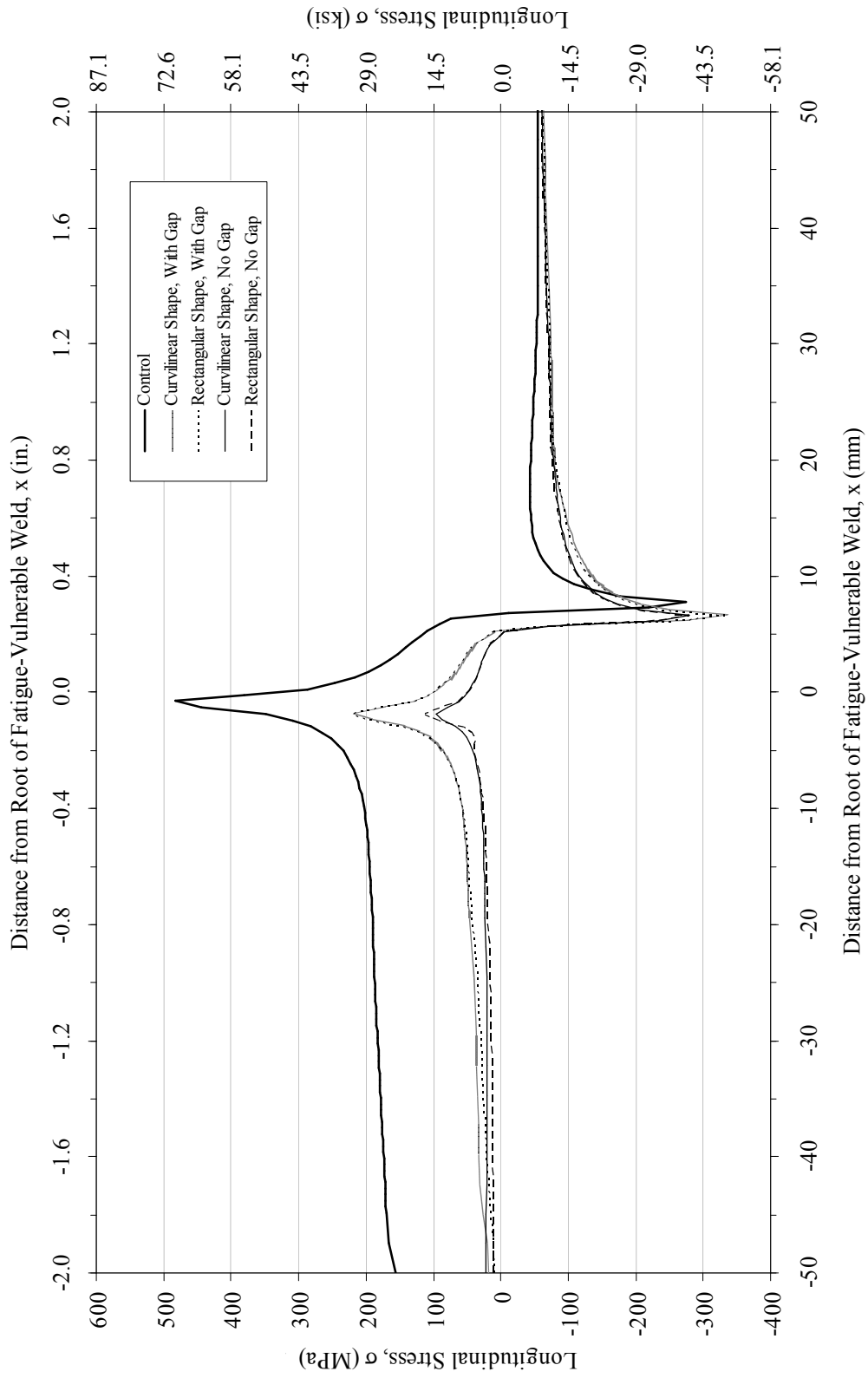


Figure 3-9. Comparison of Stress Data for Finite Element Models with CFRP Overlay Shape Varied

Figure 3-9 shows a comparison of the longitudinal stress data obtained from models with different shapes of composite overlays as detailed in Figure 3-4. A reduction in stresses in the vicinity of the weld is clearly shown for the CFRP-stiffened models when compared to the model of an unstiffened steel specimen. Additionally, it can be seen that the shape of the CFRP overlays did not significantly affect the overall stiffness of the detail (and thus the stresses at the weld). However, the presence of bonded surfaces directly adjacent to the weld had a very significant effect in decreasing weld stresses, a behavior that seems to contradict the initial assumption that the rolled plies in the CFRP overlay elements were not contributing to the strength of the composites. It is important to note that the peak stress data recovered from the finite element model is not considered to be a good representation of the peak weld stress since the model was limited to a linear-elastic analysis. Just as discussed previously for model deflection data, it is the behavior of the model that is most valuable. In this case, the behavior exhibited by the finite element models indicated that altering the shape of the CFRP overlays should not be expected to cause a significant change in the weld stress while bonding of the area directly adjacent to the weld should be expected to decrease the weld stress.

Finally, the models predicted that the relative stiffening capability of the CFRP overlays was inversely proportional to the thickness of the bond between the composite and steel materials. This result was expected in that with increased thickness, the bond material experiences less internal constraint and lower stresses (shear and principle), similar to the transition from plane stress to plane strain conditions in metallic materials. Additionally, this effect has been documented in previous research by

Colombi et al (2003). The difference between the epoxy bond material and a metal is that with a linear increase in bond thickness of the epoxy, the corresponding increase in shear strains may not necessarily be linear and can be affected greatly by environmental conditions such as temperature, or humidity.

CHAPTER 4 – FATIGUE ENHANCEMENT TESTING OF CFRP OVERLAYS

4.1. OBJECTIVE

The primary objective of the fatigue testing was to show that application of high-strength CFRP composite materials as an overlay element to fatigue-vulnerable welds is a viable method for enhancing fatigue life of the detail by increasing stiffness and reducing the stress demand. A second objective was to investigate effects of manufacturing techniques such as bond thickness, bond composition, and bond boundary conditions on the effectiveness and durability of the overlay elements.

4.2. EXPERIMENTAL SETUP

Although no longer commonly used as a retrofit, it was quite common for bridge engineers to employ welded coverplates to reinforce steel girder flanges in regions of high moment demand as recently as 40 years ago. Welding of the coverplates provided an efficient means of ensuring load transfer while minimizing shear lag. However, from a fatigue standpoint, the use of welds created innumerable crack initiation sites, especially for the welds at coverplate ends and when thick steel plate (greater than 20.3 mm (0.80 in)) was utilized. This particular detail proved to be so prone to development of fatigue cracks that AASHTO subsequently categorized it with the worst fatigue rating possible, denoted as Category E'. Despite current knowledge that this detail is a poor performer under fatigue loading, many examples can still be found in aging, existing steel bridges.

Since the aim of this research was to prove the viability of CFRP doubler elements in the enhancement of fatigue life, this Category E' (AASHTO 2007) fatigue-

vulnerable cover plate detail was chosen as the specimen to which the CFRP overlay elements would be applied. The detail's poor fatigue performance in combination with its commonality made this detail an excellent candidate for study.

4.2.1 STEEL SPECIMENS

The steel specimens to which CFRP doublers were later bonded were comprised of two 25.4 mm (1.00 in.) thick plates welded together with a 7.94 mm (5/16 in.) fillet weld as discussed in section 3.2.1. All steel specimens were A36 grade steel to best represent actual examples of this detail in aging steel bridges. One of the two plates was wider and longer than the other, with the larger representing a bottom flange of a steel girder, and the smaller representing a coverplate. Dimensions of the welded coverplate were such that the detail was categorized as an AASHTO (2007) Category E' fatigue detail. Dimensions were chosen to balance the effects of shear lag and stress distribution considerations according to St. Venant's Principle (Vilhauer 2007), and are shown in Figure 3-1.

The geometry corresponding to a Category E' detail was selected as the most appropriate for fatigue testing for several reasons. First, choosing the worst fatigue category provided the greatest opportunity for improvement. If a Category C detail had been chosen, then the greatest improvement due to fatigue enhancement that could be gained (Category A detail behavior) would be a two category improvement regardless of how much better the enhanced detail performed. However, if a Category E' detail was enhanced in such a way that it were to behave as a Category A detail, then a seven

category improvement would have occurred, which would indicate the best possible improvement. Second, as discussed previously, the geometry chosen for the specimens was a representative detail for current problems facing bridge maintenance officials. Category E' coverplates currently exist on bridges in use across the nation, and are frequently flagged for fatigue cracking issues (Vilhauer 2007).

4.2.2 CFRP OVERLAY ELEMENTS

As discussed in Chapter 3, the CFRP overlay elements were constructed by layering forty plies of bi-directional carbon-fiber fabric pre-impregnated with cyanimide-123 resin in a custom machined aluminum mold. Each layer of carbon fiber fabric was cut to a different length such that the final profile of the stack was curvilinear. Five plies of boron-fiber were included in the stack to limit out-of-plane migration of the carbon-fiber layers during the molding process, and several layers of resin film were added to eliminate voids at the step in the CFRP overlay profile.

A heat-press was utilized to produce CFRP overlays with good consolidation. The heated platens of the press applied a pressure of 18.0 bar, or 1.80 Mpa (260 psi), and a temperature of 177 °C (350 °F) to the overlay elements within the mold for three to four hours until complete cross-linking of the resin was achieved. CFRP overlays produced by this method had a curvilinear profile and approximately uniform curvature and thicknesses. Figure 3-2b shows the profile of the CFRP overlay elements utilized for the fatigue testing.

The thickness of the overlays when bonded to the steel served to increase the bending moment of inertia of the specimen around the fatigue-critical welds. The intent of the increased moment of inertia was to cause the specimen to have increased stiffness, smaller deflections, and lower stress demand at the welds. It should be noted that this approach differed from the techniques discussed in previous literature (Colombi et al).

4.2.3 CFRP-STIFFENED STEEL SPECIMENS

Bonding of the CFRP overlay elements to the steel specimens was accomplished using Hysol (Loctite 9412), a commercially-available high-grade resin epoxy. The surface of the steel substrate was prepared using a standard hand grinder and degreased using a mild acid solution and isopropyl alcohol. Composite overlay surfaces were roughened using 100-grit sandpaper and were also degreased using isopropyl alcohol. The bond between the CFRP overlay and the steel substrate was cured at room temperature for a minimum of 48 hours before any load was applied. Four steel specimens were outfitted with CFRP overlay elements, specimens TRI_02, TRI_04, TRI_05, and TRI_06. It should be noted that specimen TRI_02 is included in the fatigue testing program as a point of reference for the behavior of the CFRP-stiffened specimens as discussed in chapter 3, and the specimen TRI_03 was rejected during the testing due to excessive warpage that occurred due to improper welding techniques.

All CFRP-stiffened specimens were outfitted with composite overlays manufactured using materials and processes that were as close to identical as practically possible. The same procedure was followed each time for lay-up, molding, and curing, and the pre-impregnated carbon-fiber fabric materials and bonding resin were from the same respective companies throughout the research and testing program.

The bond thickness between each steel specimen and respective composite overlays was varied as shown in Table 4-1.

Table 4-1. Fatigue Testing Results for CFRP-Stiffened Specimens and Control Specimens

Specimen ID	Bond Thickness mm (in.)	No. of Cycles to Crack Initiation in Steel Substrate	Avg. No. of Cycles to CFRP Debond	Std. Dev. Of CFRP Debond	No. of CFRP Debondings
TRI_02*	0.76 (0.030)	460,000 [†]	275,000	n/a	1
TRI_06	1.65 (0.065)	n/a	431,500	133,500	5
TRI_04	3.18 (0.125)	1,332,000	226,600	188,000	6
TRI_05	6.35 (0.250)	n/a	1,205,000	n/a	1
Control 1	--	350,000	--	--	--
Control 2	--	500,000	--	--	--

*Specimen did not undergo rebonding procedure during testing

[†] Crack initiation based on recorded stiffness data

It was hypothesized that increased bond thickness between the steel and CFRP specimens would decrease the stiffening ability of the CFRP-overlay elements as well as decrease the frequency of overlay element debonding (Colombi et al. 2003). TRI_02 was fabricated with a bond thickness of 0.76 mm (0.030 in), TRI_06 had a bond thickness of 1.65 mm (0.065 in), TRI_04 had a bond thickness of 3.18 mm (0.125 in), and TRI_05 had a bond thickness of 6.35 mm (0.25 in).

The bonding resin used in this research has a very low initial viscosity which made the process of creating thick bonds more difficult. TRI_05 was fabricated to have 6.35 mm (0.250 in.) thick bonds, and a resin captivation material made from polyester fibers was added to the bond. This material kept the resin in place by the mechanism of capillary action, and it was hypothesized that the shear strength of the bond would be slightly improved by the presence of the fibers (Hertzberg 1996; Mallick 1993).

4.2.4 FATIGUE TESTING EXPERIMENTAL SETUP

Four CFRP-stiffened steel specimens and two unstiffened control specimens, Control 1 and 2, were subjected to fatigue loading in three-point bend test fixtures. Three-point bending was chosen as the method of load application to accommodate the size of the specimens as well as to eliminate eccentric loading that would be produced under pure tensile loads due to the asymmetric nature of the specimen.

Two test frames were utilized for the testing: an Instron model 1334 closed-loop servohydraulic test frame with a static load rating of ± 489 kN (110 kip) and a fatigue load rating of ± 240 kN (55.0 kip), and a MTS closed-loop servohydraulic test frame with a static load rating of ± 222 kN (50.0 kip) and a fatigue load rating of ± 156 kN (35.0 kip). The Instron test frame was actuated by an 8800D computer control system, while the MTS test frame was actuated by a model 880 control system. Cyclic fatigue loads for all specimens were applied such that the minimum load was one-tenth the maximum load ($R = P_{\min} / P_{\max} = 0.1$), and the maximum load applied was 17.1 kN (3.84 kip), which corresponded to a stress range at the weld toe in the control specimen

of 138 MPa (20.0 ksi). Cyclic loading was applied using a sine function at a rate of 1.5 to 2 Hz. Figure 4-1 shows a schematic drawing of the three-point bending fixture used in this testing.

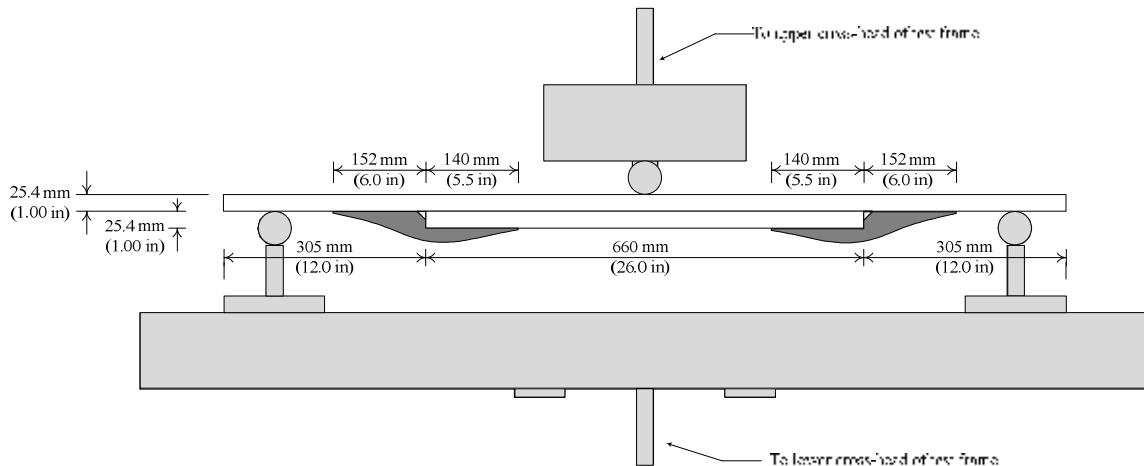


Figure 4-1. Schematic of Three-Point Bending Fixture with CFRP-Stiffened Specimen

The computer controller for the Instron test frame was used to monitor load and deflection data for each loading cycle. Maximum and minimum load and deflection data were saved to a spreadsheet file every 50th cycle. Likewise, the controller for the MTS test frame was used to monitor load and deflection continuously over the loading cycles, and the maximum and minimum load and deflection for every 50th cycle were recorded using a National Instruments LabVIEW (version 7.0) data acquisition system.

Testing on all stiffened specimens progressed until a crack initiated in the steel, one of the composite overlay elements experienced a failure in the bond to the steel, or the total number of applied fatigue cycles reached a minimum threshold of 1.5 Million cycles. For this research, this threshold was chosen to define run-out of the specimens because it corresponds to the expected crack initiation behavior of a Category B detail

subjected to a stress range of 138 MPa (20 ksi) (AASHTO 2007). In the event that a CFRP-overlay element debonded, testing of that specimen was stopped, the CFRP-overlay element was removed, and the weld to which the composite had been bonded was inspected for the presence of a crack using a dye penetrant. If no crack was detected, then the surfaces on both the CFRP-overlay element and the steel specimen were cleaned and prepared for rebonding. Once the composite was rebonded, testing was resumed. The exception to this procedure was TRI_02, for which the test was not stopped in the event of a debond, but was continued to gain perspective of the behavior of the steel after debonding of a CFRP overlay element as described in chapter 3.

Finally, two unstiffened steel specimens were tested in fatigue (Vilhauer 2007) to serve as a control group for the experimental testing. Control specimens 1 and 2 were tested at a stress range of 138 MPa (20.0 ksi) using the Instron test frame as described above, with the ratio of minimum to maximum load set at $R = 0.1$.

Finite element models were also utilized as an aid during the fatigue testing. The experimental setup for the finite element models is as described in Chapter 3, section 3.2.4

4.3. DISCUSSION OF RESULTS

Control specimens 1 and 2, each tested at a stress range of 138 MPa (20.0 ksi), demonstrated crack initiation lives of 350,000 cycles and 500,000 cycles, respectively. Three of the four fatigue tests of CFRP-stiffened steel specimens exhibited significantly longer fatigue lives than unstiffened control specimens tested at the same stress range.

In addition, all of the CFRP-stiffened steel specimens exhibited considerably smaller deflections than the control specimens. Results are summarized in Table 4-1.

It can be seen from Figure 4-2 that TRI_02 did not exhibit as much of an improvement from the control specimens as the other CFRP stiffened specimens. This is suspected to be due to the early debond of one of the CFRP overlay elements, which upon inspection was attributed to the existence of a large void in the bond resin.

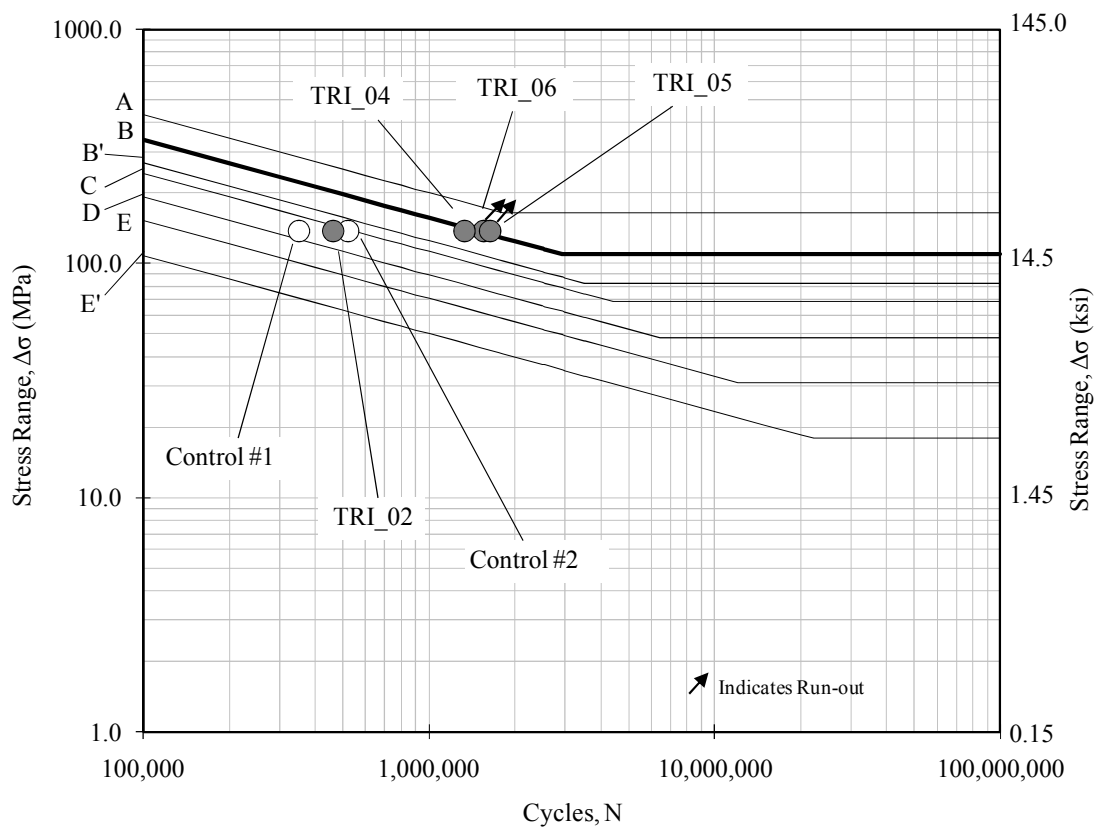


Figure 4-2. S-N Diagram of Fatigue Test Results for Experimental and Control Specimens

Additionally, rebonding of the CFRP overlays was not performed for TRI_02, and so the crack initiation life is comprised of a smaller portion of stiffened load cycles than the data for the other stiffened specimens. This approach was used for TRI_02 to

determine a baseline behavior of the specimens stiffened with the CFRP overlays. Crack initiation did not occur at all in TRI_05 and TRI_06 (for which rebonding was performed), which underscores the point that while a good bond was maintained between the CFRP overlay elements and the steel, the increased stiffness at the fatigue-vulnerable weld inhibited crack initiation for the stress range at which the specimens were tested.

Crack initiation did occur in TRI_04, and was discovered upon inspection after the specimen had been subjected to 2,052,000 cycles. The same weld had previously been inspected at 1,332,000 cycles. Weld inspection was not possible for the 720,000 cycles between examinations due to the presence of the CFRP overlay element. During testing it was observed that one of the CFRP overlay elements underwent internal degradation (delamination and cracking) that led to the overlay exhibiting decreased stiffness, which could be visibly discerned. Upon this discovery, noted at 1,125,000 cycles, the degraded overlay was removed, and a new overlay was applied. It is hypothesized that crack initiation was influenced by the presence of the degraded CFRP overlay element, but the extent of the influence could not be discerned from the data recorded. In addition, TRI_04 experienced the greatest number of debond events (six) for all of the CFRP-stiffened specimens. This relatively high frequency of debonding likely coincided with TRI_04 undergoing a greater number of unstiffened (or stiffened to a lesser degree) fatigue cycles when compared to the other experimental specimens. Given the very small size of the crack upon discovery (approximately 1.6 mm (0.063 in.)), it is surmised that initiation occurred after the 1.5 Million cycle run-out threshold, however evidence to support or dispute this hypothesis was not recorded. Thus, the

only definitive conclusion that can be presented is that TRI_04 did not exhibit crack initiation until after it was subjected to 1,332,000 cycles. While this is a large improvement over the fatigue behavior of the control specimens, it was not as great of an improvement in behavior as recorded for TRI_05 and TRI_06.

Figure 4-2 shows S-N curves for AASHTO fatigue detail categories A through E' with crack initiation fatigue life plotted for specimens TRI_02, TRI_04, TRI_05, and TRI_06. Specimens TRI_04, TRI_05, and TRI_06 all exhibited behavior at or above the curve expected for an AASHTO Category B' detail, and Specimens TRI_05 and TRI_06 exhibited behavior at or above the curve expected for an AASHTO Category B detail. The control specimens exhibited behavior between Categories D and C, and Specimen TRI_02 exhibited behavior that fell between the two control specimens.

4.3.1 EFFECTS OF BOND THICKNESS ON CFRP OVERLAY EFFECTIVENESS

One of the initial hypotheses set forth in this research was that increased bond thickness between the steel and CFRP elements would increase the bond tenacity while some stiffening capability would be sacrificed. A decrease in the frequency of debond was predicted from results of finite element models that showed a decrease in peak shear stress within the bond material as the thickness of the bond was increased. Figure 4-3 shows shear stress along the bonded surface of the CFRP overlay for bond thicknesses varying from 0.8 mm (0.03 in.) to 3.2 mm (0.13 in.) (F. Alemdar, unpublished internal report, December 2007). In all cases modeled, the maximum shear stress in the bond decreased as the thickness was increased.

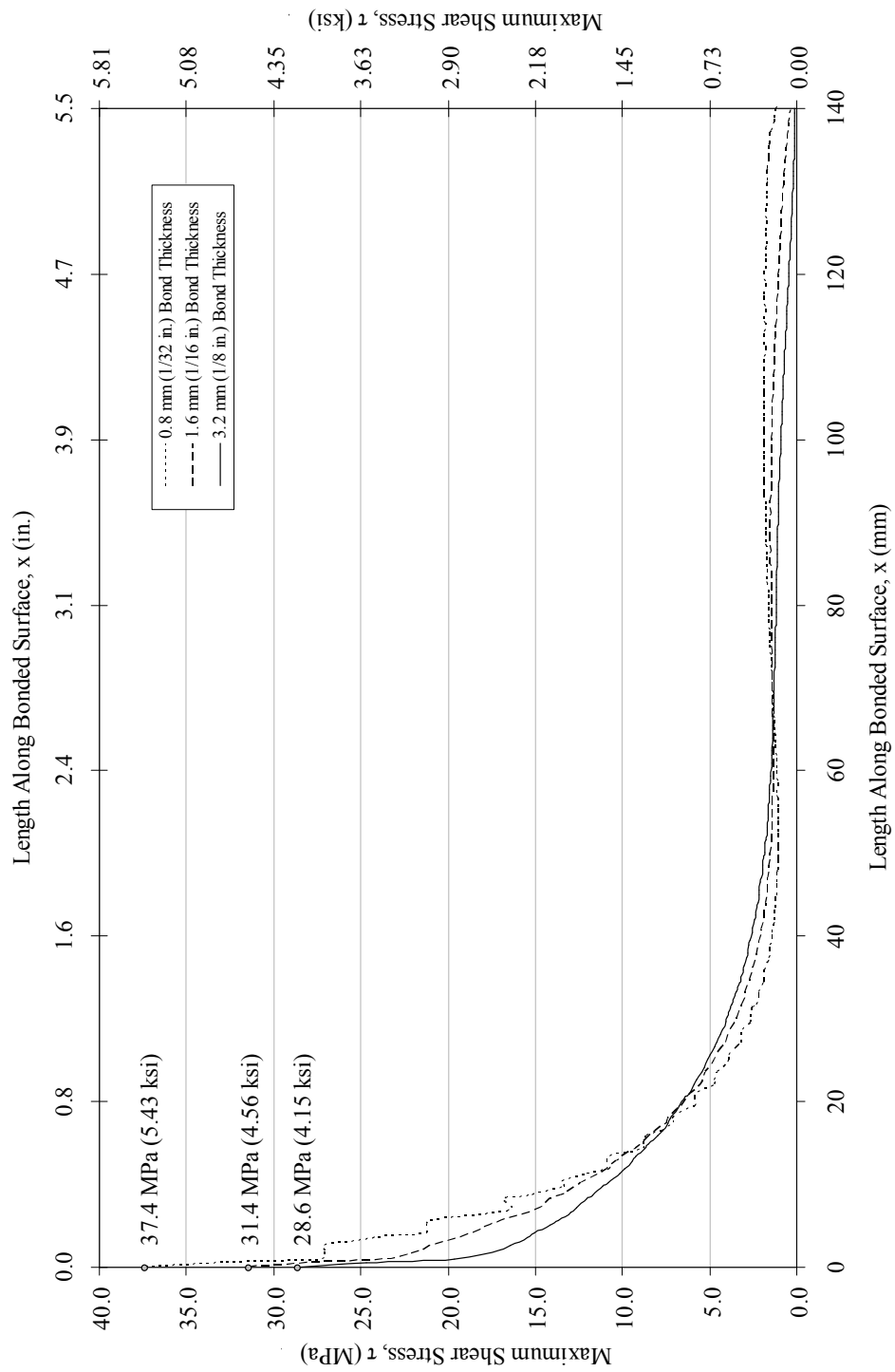


Figure 4-3. Shear Stress for Varied Bond Thickness from Finite Element Models

The importance of shear stresses at the leading edge of the bond was further confirmed through experimental observation that the bond failure path propagated through the bond material to the leading edge at an angle of approximately 45° as shown in Figure 4-4. A goal of the testing in light of the hypothesis presented above was to determine an optimal bond thickness that provided enough stiffness to the specimen to increase the life of the fatigue-vulnerable welds while still minimizing the shear stress in the bond material, thus minimizing the frequency of debonding of the CFRP-overlay elements from the steel specimens.

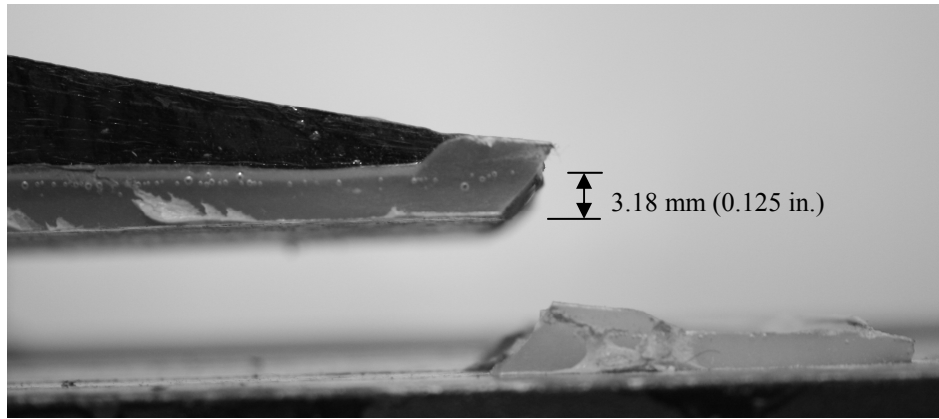


Figure 4-4. Close-up View of Leading Edge of a Debonded CFRP Overlay Element

One parameter examined from test results of the stiffened specimens was the instantaneous stiffness, or dynamic stiffness of the specimens. In this research, dynamic stiffness was defined as the change in the applied load divided by the change in deflection of the specimen for each recorded fatigue cycle:

$$K_{\text{dyn}} = \Delta P / \Delta y \quad (1)$$

where,

ΔP = the change in applied load over one fatigue cycle

Δy = the change in deflection over one fatigue cycle

A decrease in the dynamic stiffness of the specimen served as an indication of change in specimen response to load. This change was either due to the initiation and propagation of a crack in the steel or initiation and progression of a debonding failure at either of the bonded CFRP-overlay element locations. It was not difficult to differentiate between the two stiffness reduction mechanisms. Changes in stiffness due to crack initiation and propagation in the steel substrate occurred over multiple hundreds of thousands of cycles, while changes in stiffness due to debonding occurred in less than ten thousand cycles.

Figure 4-5 displays dynamic stiffness data determined for each of the four specimens tested, as well as for the two control specimens. The values shown are the average of the dynamic stiffness data recorded at fifty cycle intervals during testing of the specimens. For the CFRP stiffened specimens, this dynamic stiffness data excludes load cycles in which the CFRP overlay was undergoing debond, thus representing the stiffened specimen stiffness.

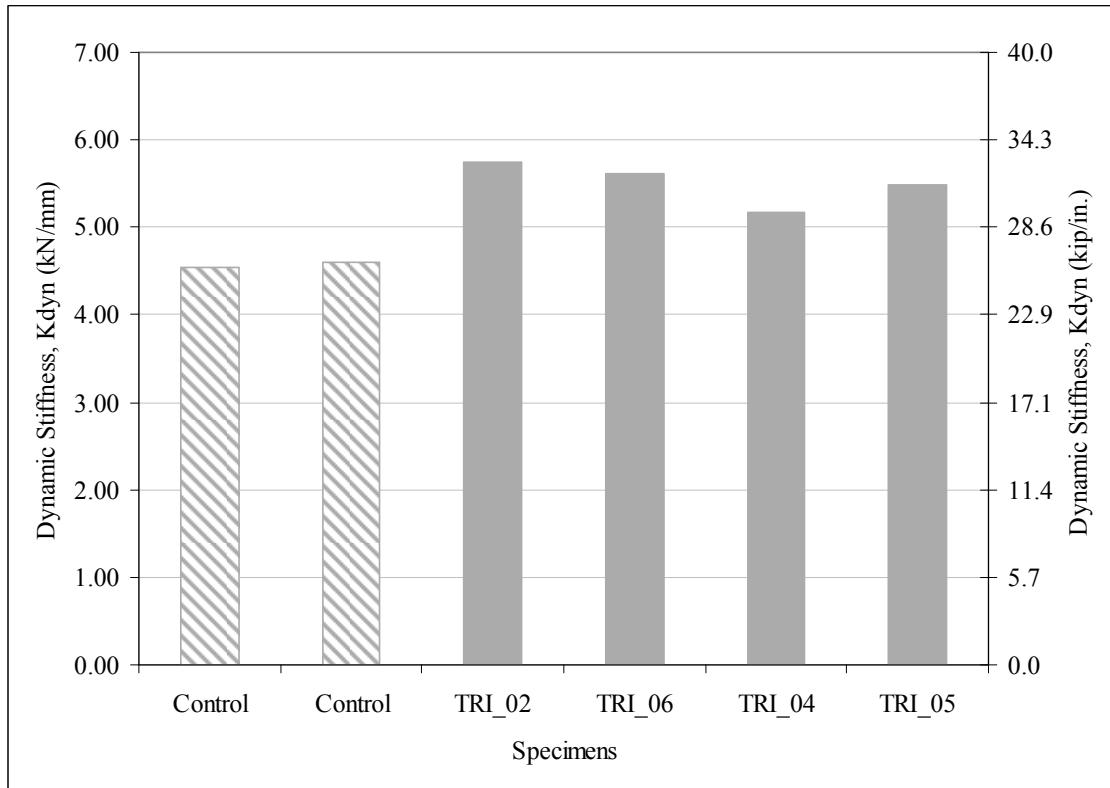


Figure 4-5. Dynamic Stiffness of CFRP-Stiffened Steel Specimens

It should be noted that data for TRI_05 did not follow the trend for TRI_02, TRI_04, and TRI_06. The presence of the resin captivation layer is surmised to have noticeably improved the shear strength of the bond from that of the epoxy resin alone to that of a polyester fiber reinforced polymer material (albeit one with a lower than normal fiber volume fraction).

Additional explanation as to why the dynamic stiffness of TRI_05 did not follow the trend of the other specimens is likely due the effect of the increased bond thickness on the moment of inertia of the specimen in the region of the weld. As can be seen from the data in Table 4-1, bond thicknesses were doubled as testing progressed. However, all CFRP-stiffened specimens demonstrated dynamic stiffnesses greater than

that measured for the control specimens. Thus, the initial hypothesis that the stiffening effect of the CFRP overlays would decrease with increasing bond thickness was only partially correct because the effects of the thickness of the bond on the moment of inertia of the specimen near the fatigue-vulnerable weld and the presence of the resin captivation material were not considered.

4.3.2 EFFECTS OF BOND CHARACTERISTICS ON FREQUENCY OF DEBONDING

The frequency of debond for CFRP-stiffened specimens TRI_04, TRI_05, and TRI_06 is presented in Table 4-1. Specimen TRI_02 is denoted with an asterisk in Table 4-1 due to the fact that rebonding of the composite was not performed during that test. Based on the data, the original hypothesis put forth that frequency of debond would decrease with increasing bond thickness does not appear to have been correct. However, the contrast between the behavior of TRI_05 and the other specimens is quite apparent, as the CFRP overlay elements remained bonded to TRI_05 for more than 1.2 million cycles. This is believed to be primarily attributable to the effect the resin captivation layer had on the shear strength of the bond.

Additionally, it was observed during testing that if a pool of resin was left at the ends of the CFRP overlay elements during bonding, those specimens exhibited a lower debonding frequency than if the bond was trimmed to the overlay edge. It is surmised that the pool of resin acted much like a rounded fillet on the shoulder of a bar that has

been reduced in diameter, effectively reducing the stress concentration at the change in thickness of the material.

Thus, based on observations of the tests performed for this research, use of a fibrous resin captivation layer and extending the bond beyond the dimensions of the overlay was recommended for improved bond tenacity. Additionally, based on the experimental evidence collected, a bond thickness of 6.4 mm (0.25 in.) when combined with a resin captivation layer provided an optimal balance of stiffness and bond tenacity with respect to the fatigue enhancement capabilities of the CFRP overlay elements studied.

CHAPTER 5 – CONCLUSIONS AND RECOMMENDATIONS

5.1. CONCLUSIONS AND RECOMMENDATIONS

Incorporation of fatigue enhancement techniques into modern bridge design and inspection is becoming a necessity due to the large number of older steel structures in use that are exhibiting fatigue cracking. CFRP materials can exhibit excellent strength and durability characteristics when manufactured to a high standard of quality, making them ideal for use in fatigue enhancement applications. Results of the investigation presented in this thesis on the development and utilization of CFRP overlay elements for the purpose of reducing stress demand at fatigue-vulnerable welds in steel bridge girders have shown that:

- Development of CFRP overlay elements having the necessary characteristics to reduce stresses at fatigue-vulnerable welds is possible.
- Application of CFRP overlay elements to welded steel specimens increased the overall stiffness of the specimens, and the composite overlays were capable of providing stiffening for a significant number of fatigue cycles.
- Use of CFRP overlay elements that have sufficient stiffness, consolidation, and thickness to increase the overall stiffness of the structural member and reduce the stress demand at fatigue-vulnerable details can significantly increase the fatigue life of bridges and other structural systems.
- The behavior of the CFRP-stiffened steel specimens was predicted and corroborated by finite element modeling.

- Modeling results suggested that composite overlay shape (rectilinear vs. curvilinear) has a negligible effect on the stiffening effect provided to the steel specimen.
- Modeling results showed that the CFRP overlay element became more effective at reducing stresses in the weld region when the bond layer between steel and CFRP was extended as close to the weld as possible.
- Use of CFRP overlay elements to increase stiffness and reduce stress demand at fatigue-vulnerable welds had the effect of enhancing the detail by inhibiting crack initiation.
- Application of CFRP overlay elements improved the behavior of Category E' fatigue details to that of Category B' (Specimen TRI_04) and Category B (Specimens TRI_05 and TRI_06).
- The fatigue enhancement capability of the CFRP overlay elements was contingent upon a good bond between the composite and steel materials, shear resistance of the bond material, and internal integrity of the overlay composite.
- CFRP overlay elements were capable of stiffening steel specimens for a significant number of fatigue cycles. The first debond for Specimen TRI_05 occurred after 1.2 million cycles, which was more than double the crack initiation life exhibited by two control specimens.
- Addition of a polyester fiber resin captivation layer to the bond enhanced the shear strength of the bond between the CFRP overlay elements and the steel.
- Extending the resin bond beyond the interface between the steel substrate and CFRP overlay element improved bond tenacity.

The results of an investigation to study the effects of CFRP overlays showed that use of CFRP materials to enhance the fatigue performance of existing structures is a promising and viable technology. It is strongly recommended based on the findings of this research and on subsequent unreported testing that further fatigue testing be performed using the CFRP overlays bonded to the category E' details with a 3.18 mm (0.125 in.) bond containing a polyester fiber resin captivation layer. Additionally, future research in this area should investigate the applicability of CFRP composite materials for fatigue enhancement of a broader range of geometries and examine practical matters associated with field application practices. Further investigation of the effect of the fibrous resin captivation layer on the bond strength of resin epoxy as well as effects of extending the resin pool should also be performed.

REFERENCES

AASHTO (2007), *LRFD Bridge Design Specifications*, 4th Ed., American Association of State Highway and Transportation Officials, Washington, D.C.

ASTM D3039 (2000), “Standard Test Method for Tensile Properties of Polymer Matrix Composite Materials”, ASTM International, West Conshohocken, PA.

Barsom, J, Rolfe, S., (1999) *Fracture and Fatigue Control in Structures*, 3rd Ed. ASTM, West Conshohocken, PA

Bassetti, A., Nussbaumer, A., and Hirt, A. (2000) “Crack Repair and Fatigue Life Extension of Riveted Bridge Members using Composite Materials.” *Bridge Engineering Conference (IABSE)*, Sharm El-Sheikh, Egypt, Vol. I, 227-238.

Bassetti, A., Nussbaumer, A., and Hirt, A. (2000) “Fatigue Life Extension of Riveted Bridge Members using Prestressed Carbon Fibre Composites.” *Steel Structures of the 2000s (ECCS)*, Istanbul, Turkey, 375-380.

Bassetti, A., Nussbaumer, A., and Colombi, P. (2000) “Repair of Riveted Bridge Members Damaged by Fatigue using CFRP Materials.” *Advanced FRP Materials for Civil Structures*, Bologna, Italy, 33-42.

Colombi, P., Bassetti, A., and Nussbaumer, A. (2003) "Analysis of Cracked Steel Members Reinforced by Pre-stressed Composite Patch." *Fatigue Fract. Engng. Mater. Struct.*, 26, 59-66

Colombi, P., Bassetti, A., and Nussbaumer, A. (2003) "Crack Growth Induced Delamination on Steel Members Reinforced by Prestressed Composite Patch." *Fatigue Fract. Engng. Mater. Struct.*, 26, 429-437

Hertzberg, R. W. (1996), *Deformation and Fracture Mechanics of Engineering Materials*, 4th Ed., John Wiley & Sons, New York, NY

Jones, S., Civjan, S. (2003) "Application of Fiber Reinforced Polymer Overlays to Extend Steel Fatigue Life." *Journal of Composites for Construction*, 7(4), 331-338

Mallick, P. K. (1993) *Fiber-Reinforced Composites: Materials, Manufacture, and Design*, 2nd Ed., Marcel Dekker, New York, NY.

Meier, U. (1992) "Carbon fibre-reinforced polymers: Modern materials in bridge engineering." *Struct. Engng. Int.*, 1(92), 7-12.

Nozaka, K., Shield, C., Hajjar, J. (2005) "Design of a Test Specimen to Assess the Effective Bond Length of carbon Fiber-reinforced polymer strips bonded to fatigued steel bridge girders." *Journal of Composites for Construction*, 9(4), 304-312

Nozaka, K., Shield, C., Hajjar, J. (2005) “Effective Bond Length of Carbon-fiber-reinforced Polymer Strips Bonded to Fatigued Steel Bridge I-girders.” *Journal of Composites for Construction*, 10(2), 195-205

Statnikov, E. (2004) “Physics and Mechanisms of Ultrasonic Impact Treatment.” *IIW Document XIII-2004-04*, International Institute of Welding, Paris, France.

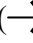



Statnikov, E. (2005) “Improvement of Quality and Reliability of Structures by means of UIT Esonix.” *IIW Document XIII-2049-05*, International Institute of Welding, Paris, France.

Vilhauer, B. (2007) “Fatigue Behavior of Welded Connections Enhanced by UIT and Bolting” thesis, presented to the University of Kansas at Lawrence, KS, in partial fulfillment of the requirements of the degree of Master of Science in Civil Engineering.

APPENDIX A

SPECIMEN TEST DATA

A1.1 INTRODUCTION

In this appendix test data recorded for the five specimens tested during this research is presented. For each specimen, an S-N plot and a dynamics stiffness plot is provided. For the S-N plots, debonding of the CFRP overlays is denoted by a small arrow (). Cycles during testing at which crack initiation occurred are denoted by the large gray-filled circle (). The end of each test is denoted by the small solid black circle (), and for specimens that did not experience crack initiation upon reaching the target testing cycle count (deemed run-out in this research), a large arrowhead is shown next to the end of test symbol (). For the dynamic stiffness plots, the control specimen stiffness was determined to be 4.56 kN/mm (926 kip/in.). Sudden changes in the dynamic stiffness of a specimen indicates debonding (and rebonding for specimens TRI_04, TRI_05, and TRI_06), and gradual changes in dynamic stiffness indicate crack growth (either in the steel or in the composite materials).

Specimen TRI_03 was rejected due to excessive warpage in the steel, and so no test results were recorded.

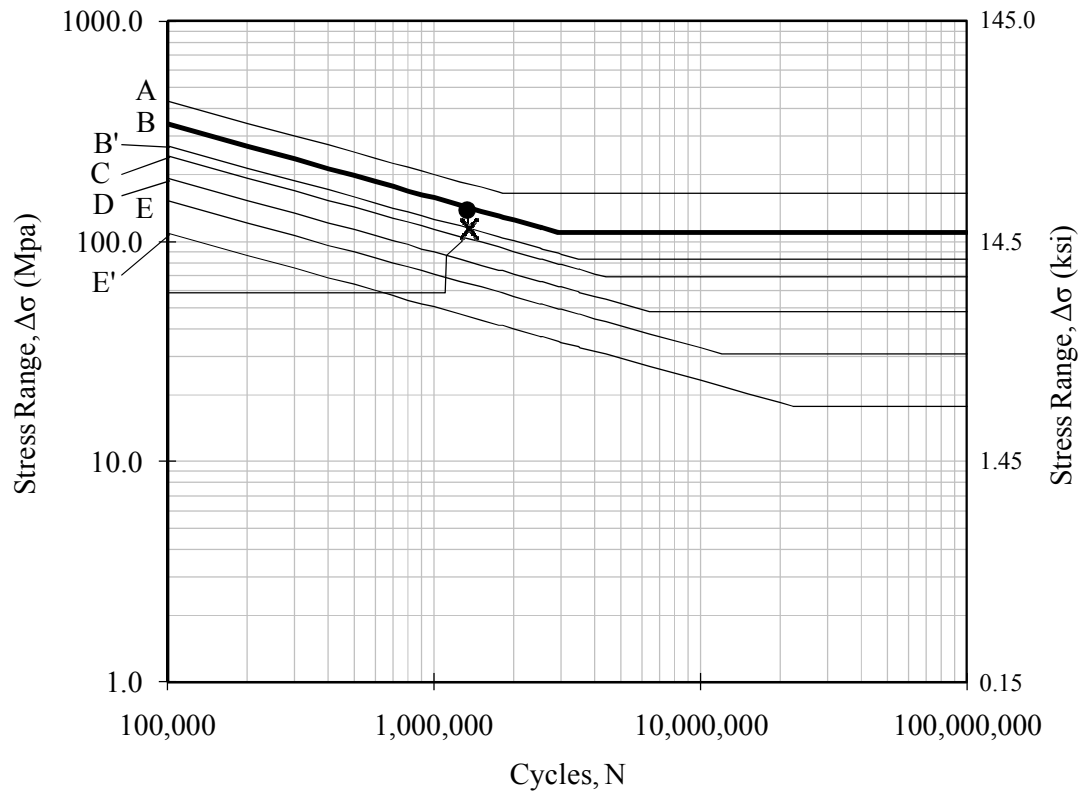


Figure A-1. S-N Data for Specimen TRI_01

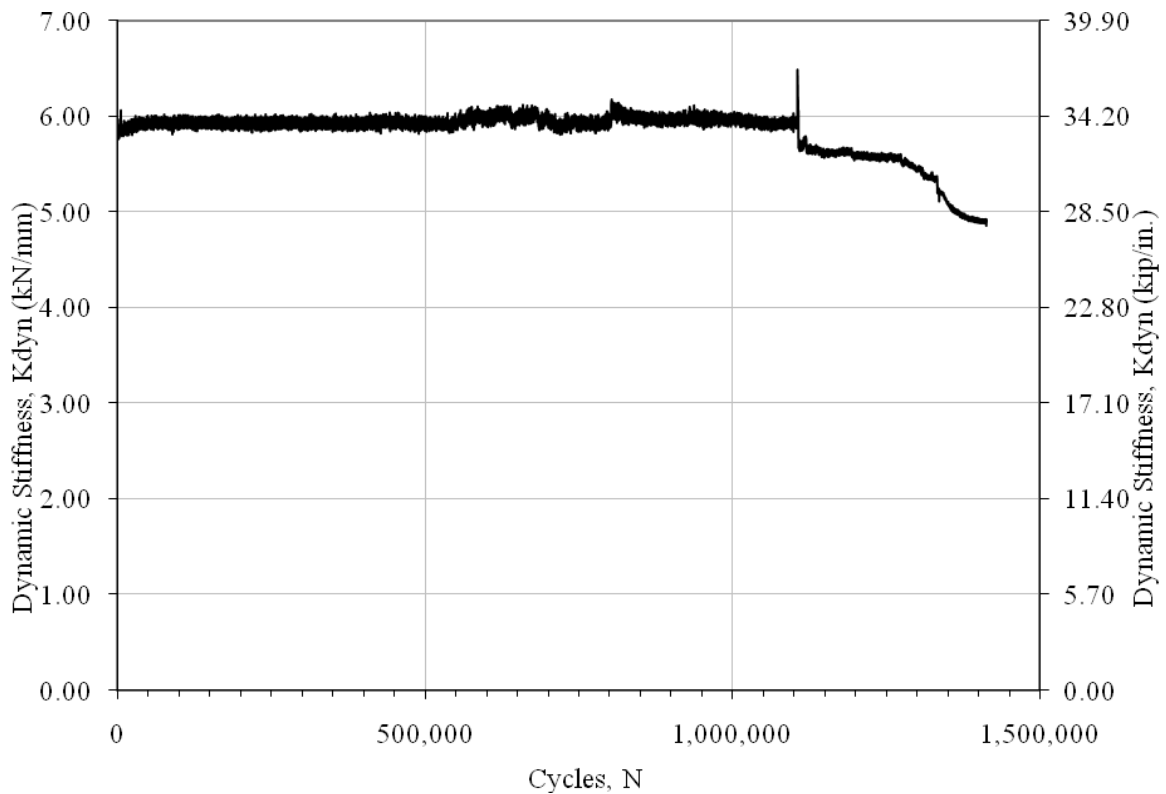


Figure A-2. Dynamic Stiffness Data for Specimen TRI_01

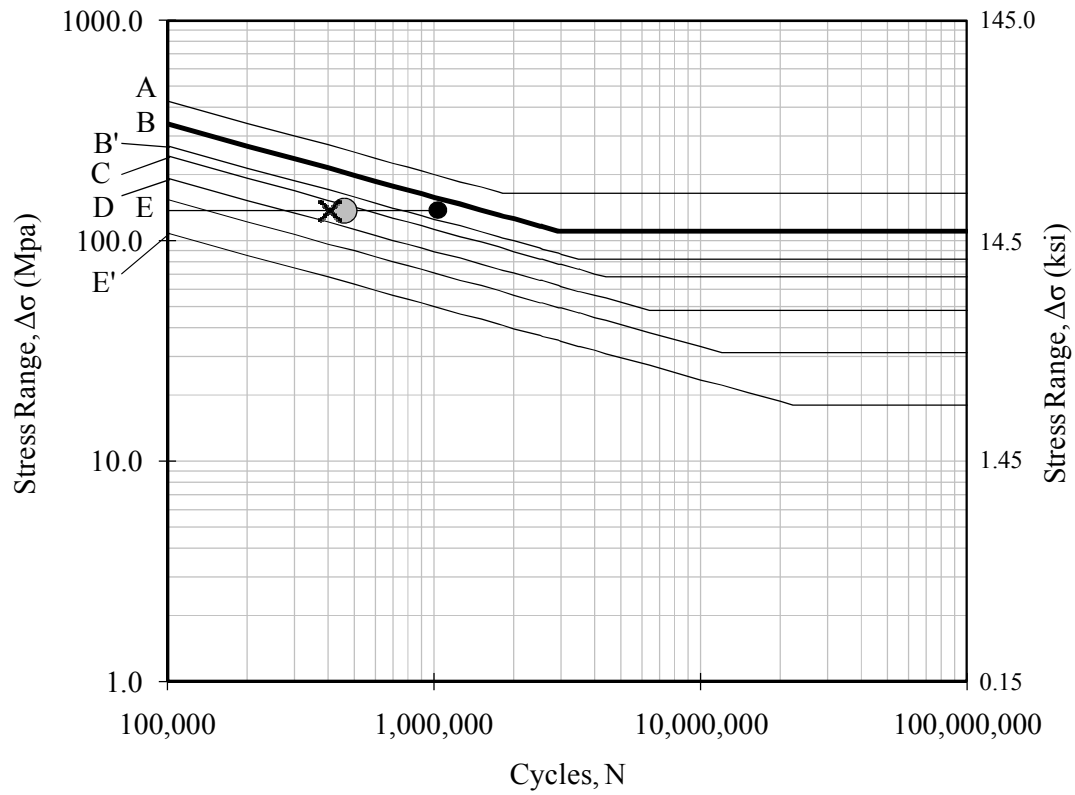


Figure A-3. S-N Data for Specimen TRI_02

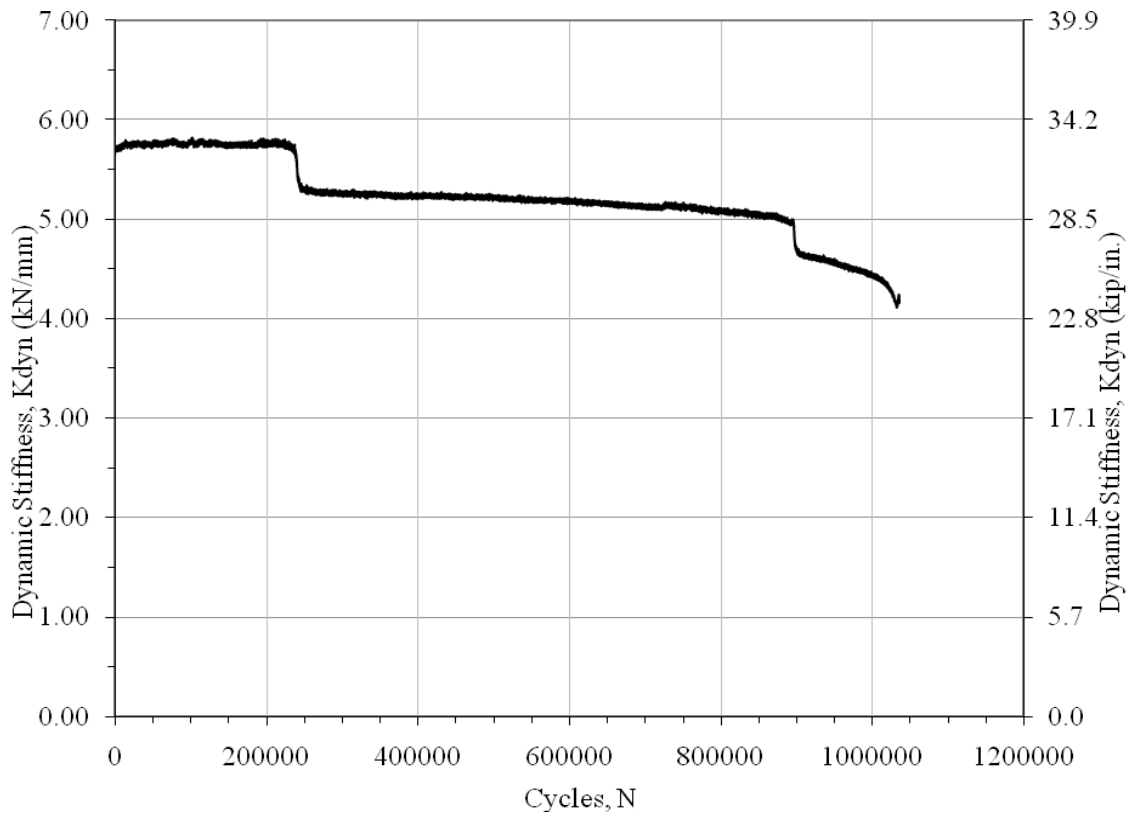


Figure A-4. Dynamic Stiffness Data for Specimen TRI_02

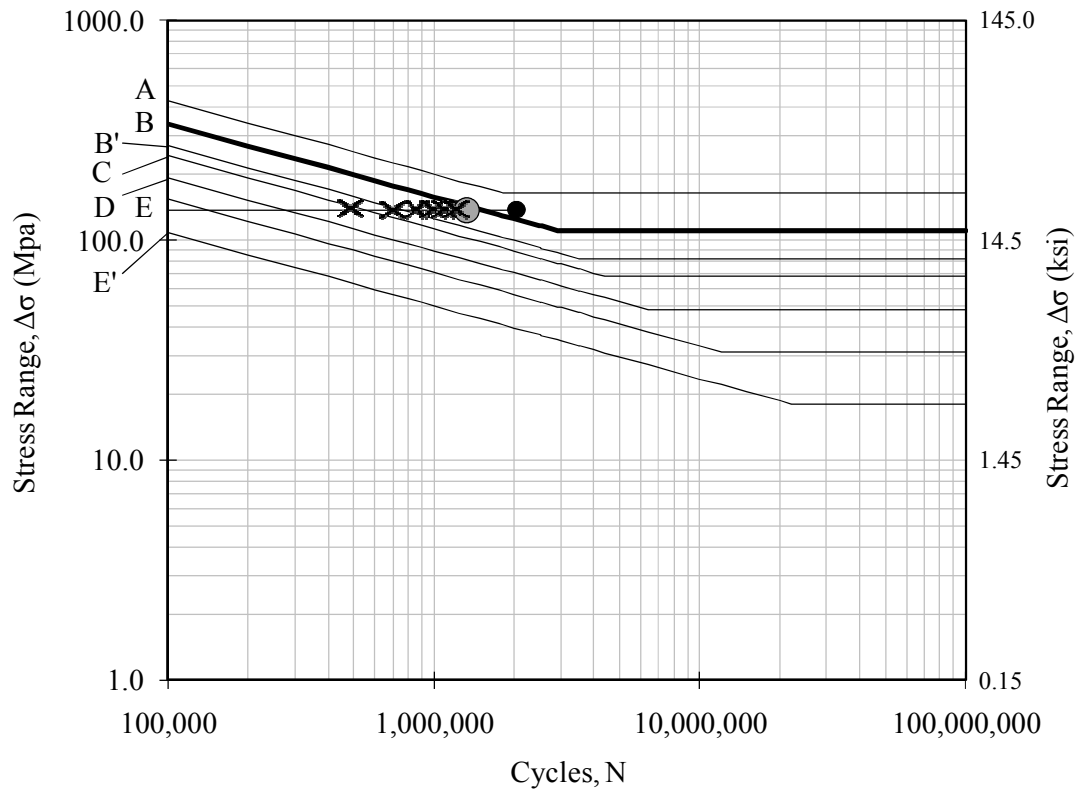


Figure A-5. S-N Data for Specimen TRI_04

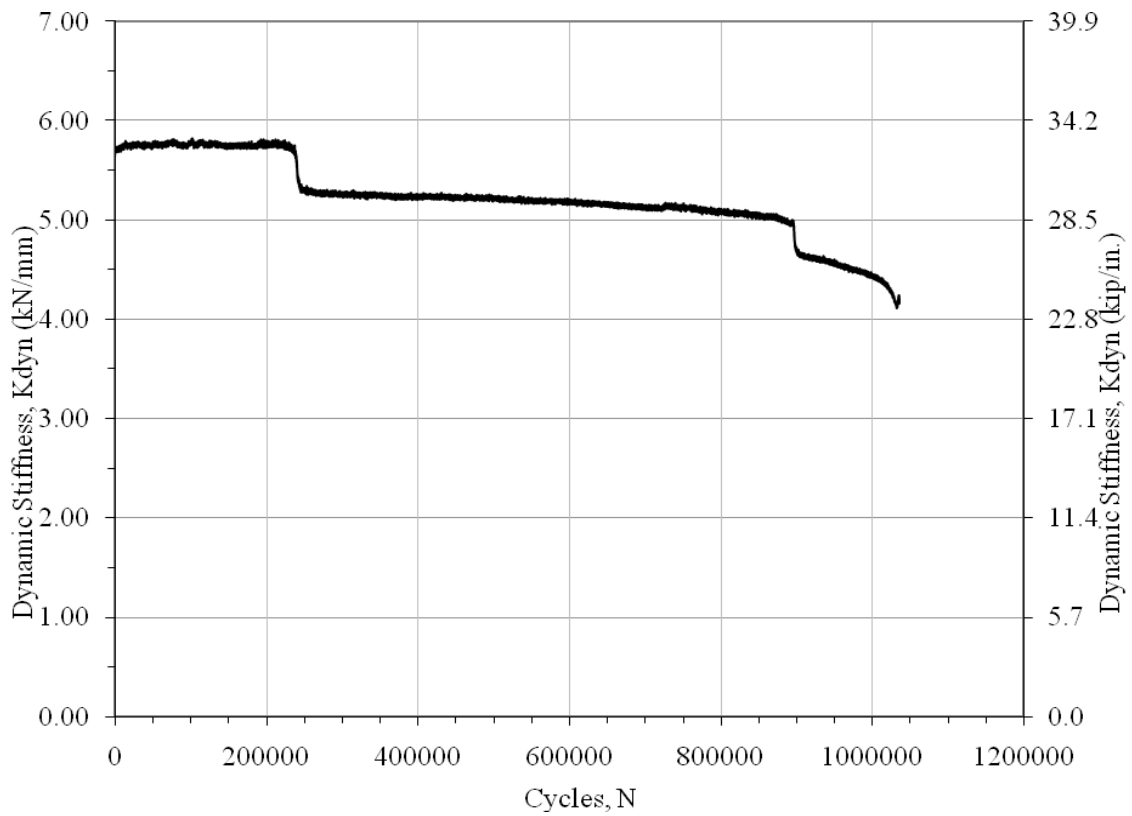


Figure A-6. Dynamic Stiffness Data for Specimen TRI_04

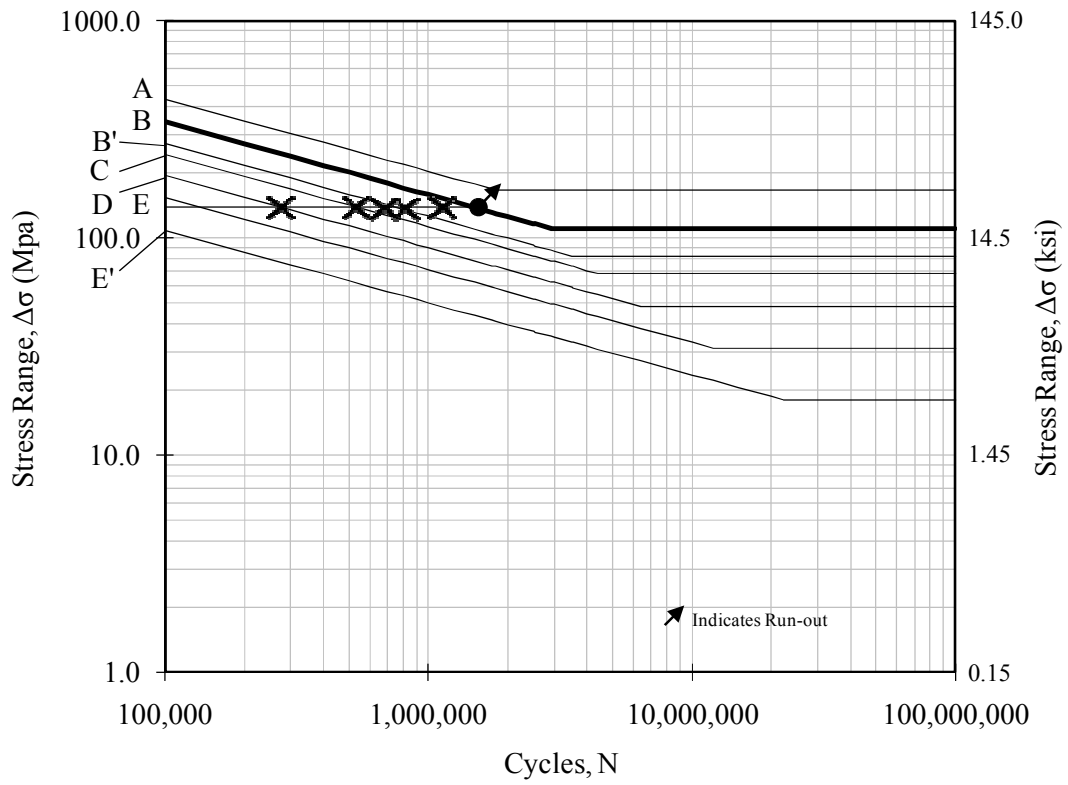


Figure A-7. S-N Data for Specimen TRI_05

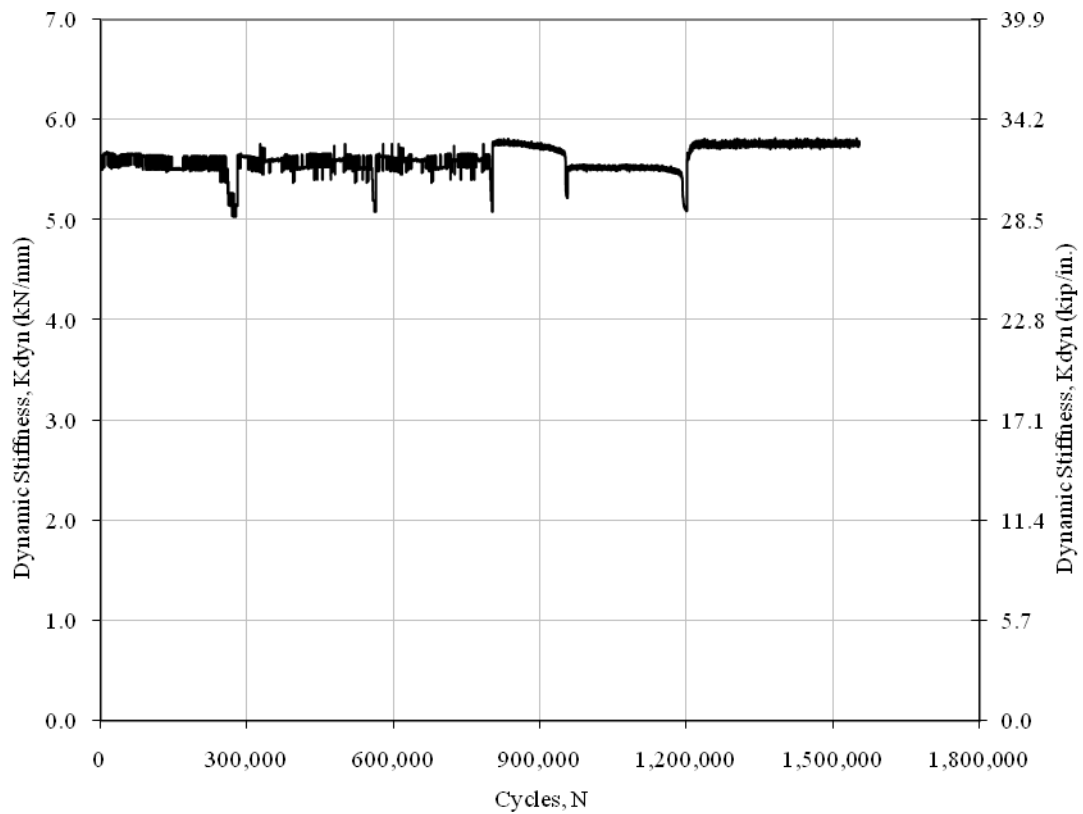


Figure A-8. Dynamic Stiffness Data for Specimen TRI_05

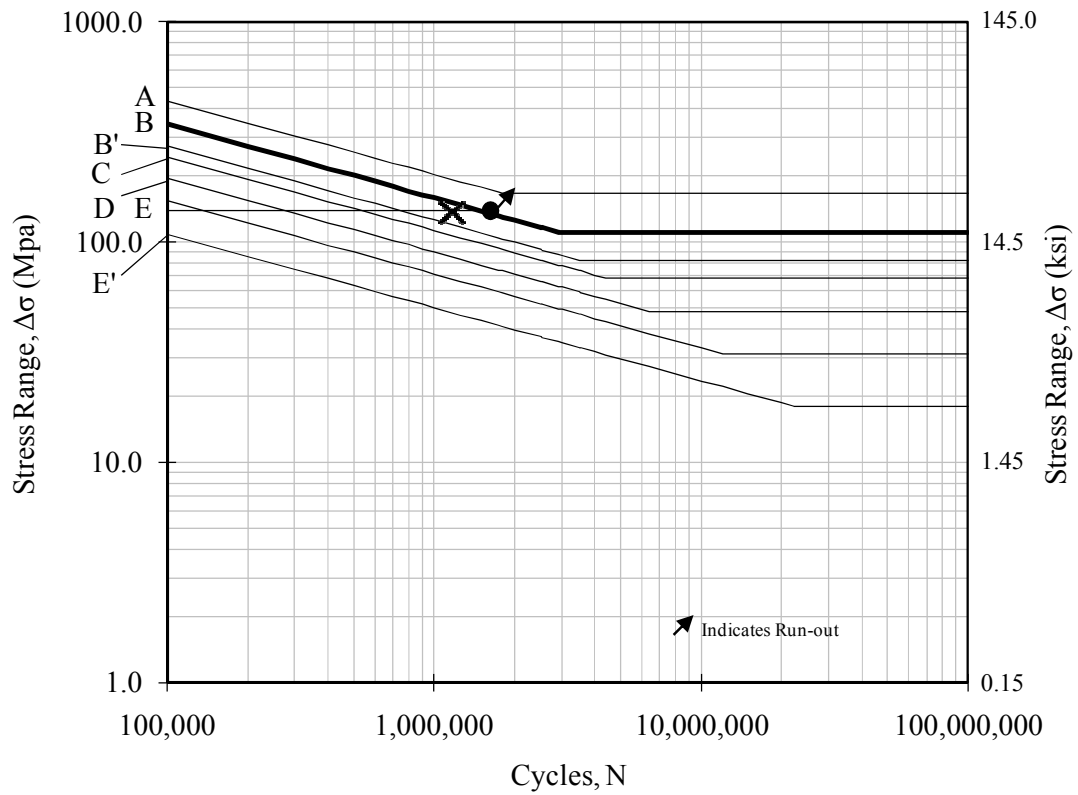


Figure A-9. S-N Data for Specimen TRI_06

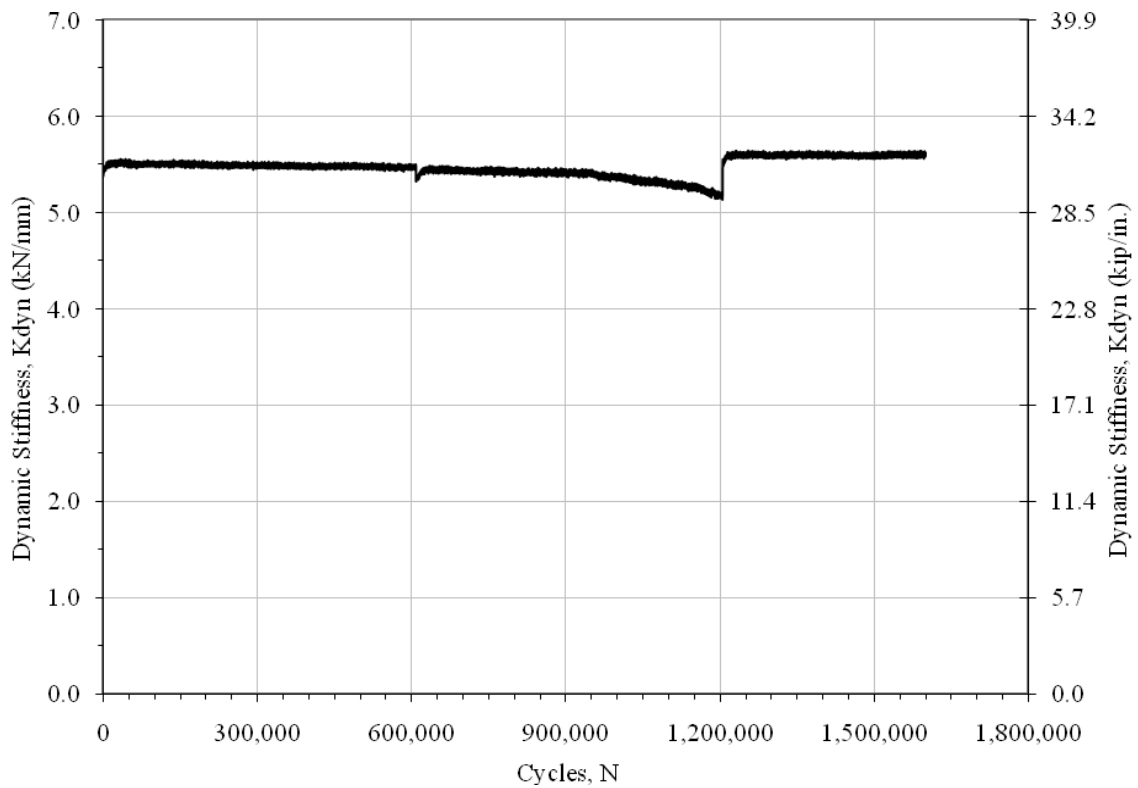


Figure A-10. Dynamic Stiffness Data for Specimen TRI_06

APPENDIX B

INSTRUCTIONS FOR MANUFACTURE AND BONDING OF CFRP OVERLAYS

B1.1 INSTRUCTIONS FOR MANUFACTURE OF CFRP OVERLAYS

A very large portion of the effort in this research was applied to the development of the CFRP overlays, and the best method to manufacture them. The following instructions detail the material preparation, lay-up, molding, unmolding, and post processing of the overlays.

B1.1.1 MATERIAL PREPARATION

The list of materials to be used for lay-up of the CFRP overlays utilized in the research described in this thesis is as follows:

1. Bi-directionally woven carbon fiber fabric strips pre-impregnated with cyanamide-123 resin at 3.75 in. in width and of the following lengths:
 - a. 1 @ 42 in.
 - b. 1 @ 22 in.
 - c. 6 @ 12 in.
 - d. 5 @ 11 in.
 - e. 5 @ 10 in.
 - f. 5 @ 9 in.
 - g. 5 @ 8 in.
 - h. 5 @ 7 in.
 - i. 9 @ 6 in.
2. Five plies of boron fibers pre-impregnated with cyanamide-123 resin at 3.75 in. in width and 11 in. in length
3. Standard resin film strips at 3.75 in. in width and the following lengths:
 - a. 1 @ 2 in.
 - b. 1 @ 4 in.
 - c. 2 @ 11 in.

Additionally, the following tools and appurtenances were required for manufacture of the CFRP overlays:

- (1) Six part aluminum mold machined to the shape of the step between the baseplate and coverplate of the steel specimens tested as part of the research described in this thesis, along with eight lengths of 3/8 in. diameter threaded rod with nuts and washers and two 1/4-20-UNC cap screws with washers. For this research the mold was coated on the inner surfaces prior to assembly with a Teflon-coated fiberglass tape to act as a release agent once the molding process was complete.
- Vacuum bag sealing mastic (will be used as a gasket material in the mold).
- (1) Industrial heat press capable of applying a minimum of fourteen tons of force and with platens capable of reaching temperatures of 350 °F.
- (1) Custom molded former block to create the curved shape on the upper surface of the overlays.
- Nylon vacuum bag material capable of resisting a minimum temperature of 350 °F, and (1) aluminum catch pan.
- Sealing tape capable of resisting a minimum temperature of 350 °F.
- (1) Rubber mallet.
- Personal protective equipment including safety glasses, latex or similar gloves, and lab apparel.

B1.1.2 CFRP OVERLAY LAY-UP

1. Coat the surfaces of the mold parts that will be internal with Teflon-coated fiberglass tape. Personal protective equipment should be in place.
2. Begin the lay-up procedure by assembling the aluminum mold. Figure B-1 shows the proper location of the vacuum bag sealing mastic on the mold base to be used as a gasket in the assembled mold.

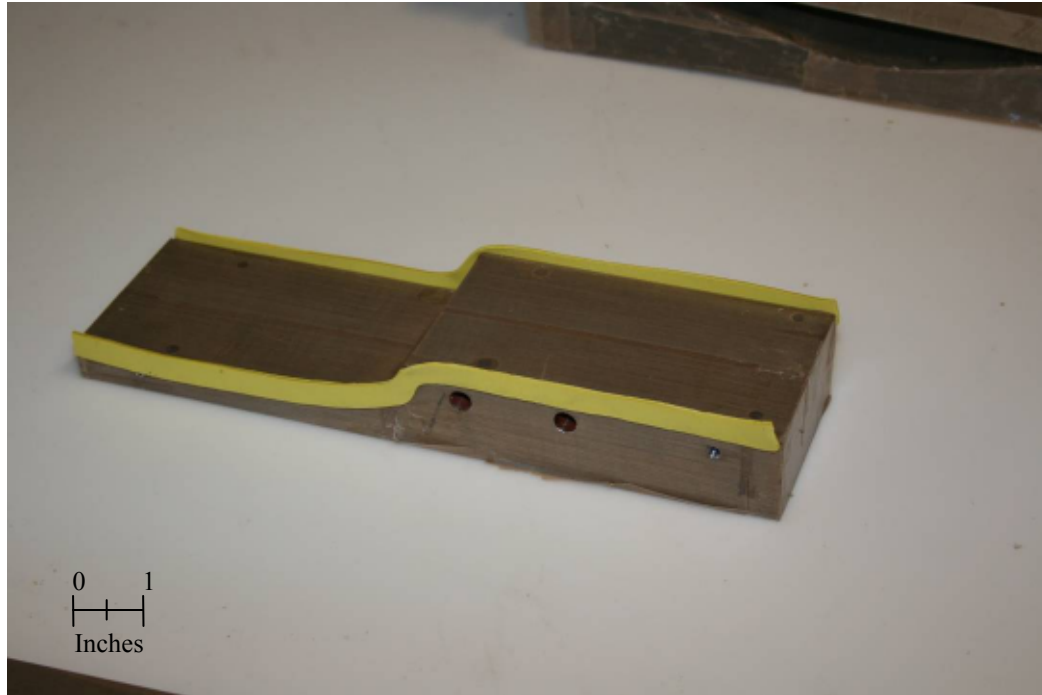


Figure B-1. Mold Base with Gasket Material

3. Figures B-2 and B-3 show the placement of one side and the ends of the mold body. The second side will need to be positioned with the aid of the rubber mallet.

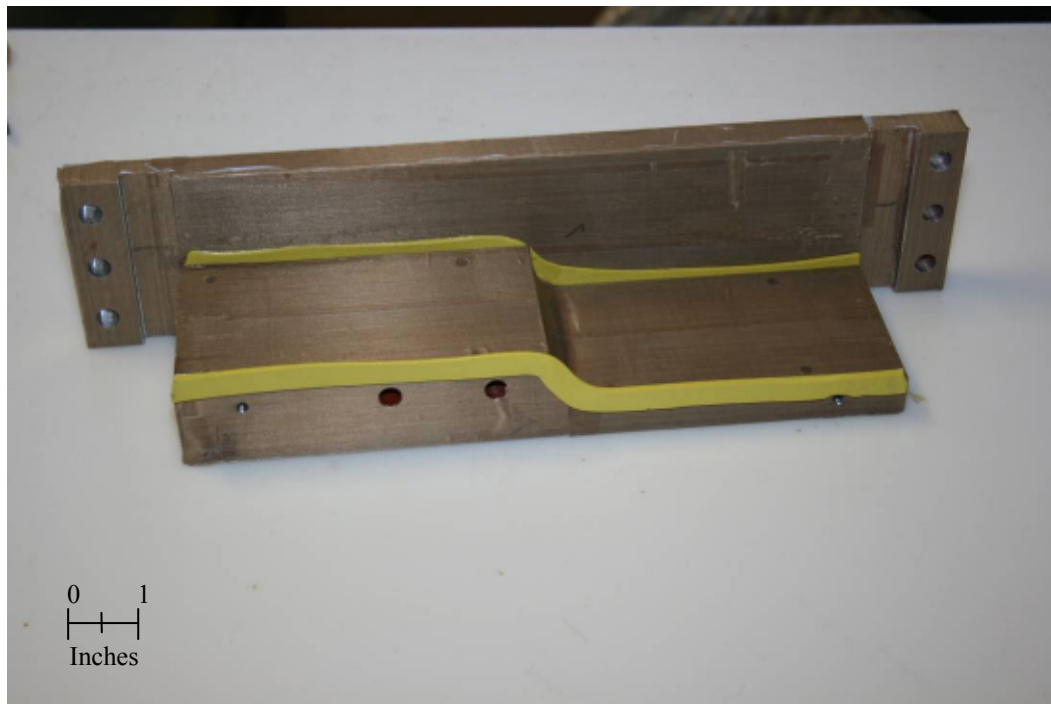


Figure B-2. Mold Base with Sidewall

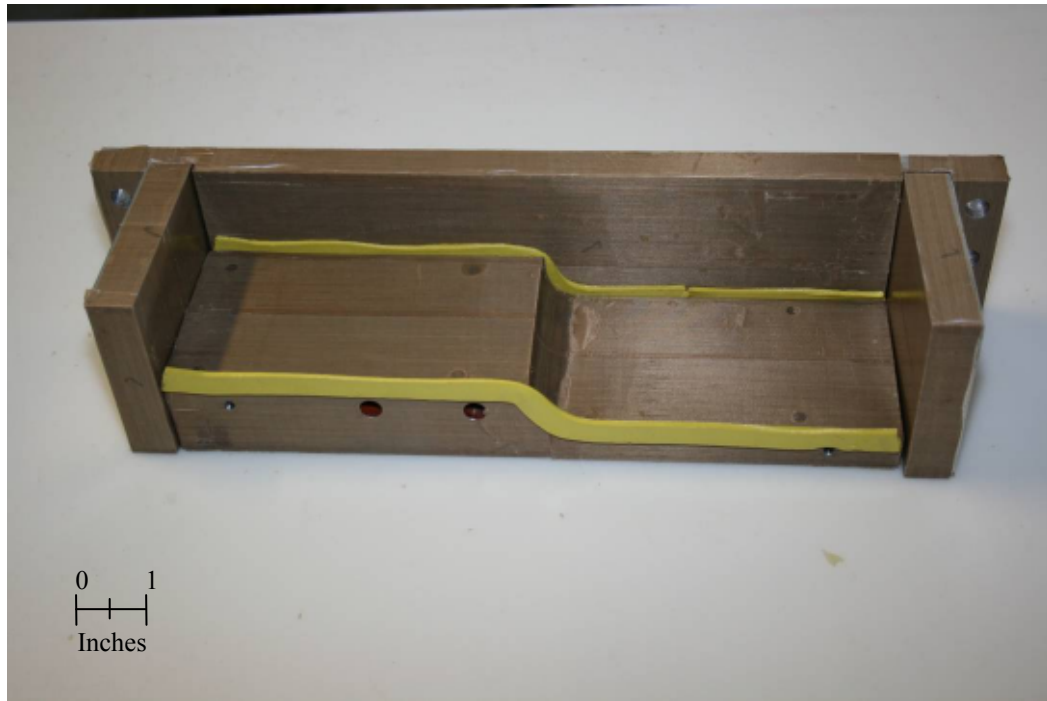


Figure B-3. Mold Base with Sidewall and Ends

4. Figure B-4 shows the mold sidewalls and ends in their proper positions. The $\frac{1}{4}$ -20-UNC cap screws with washers should be inserted and tightened (Figure B-4) prior to inserting the threaded rods with nuts and washers.

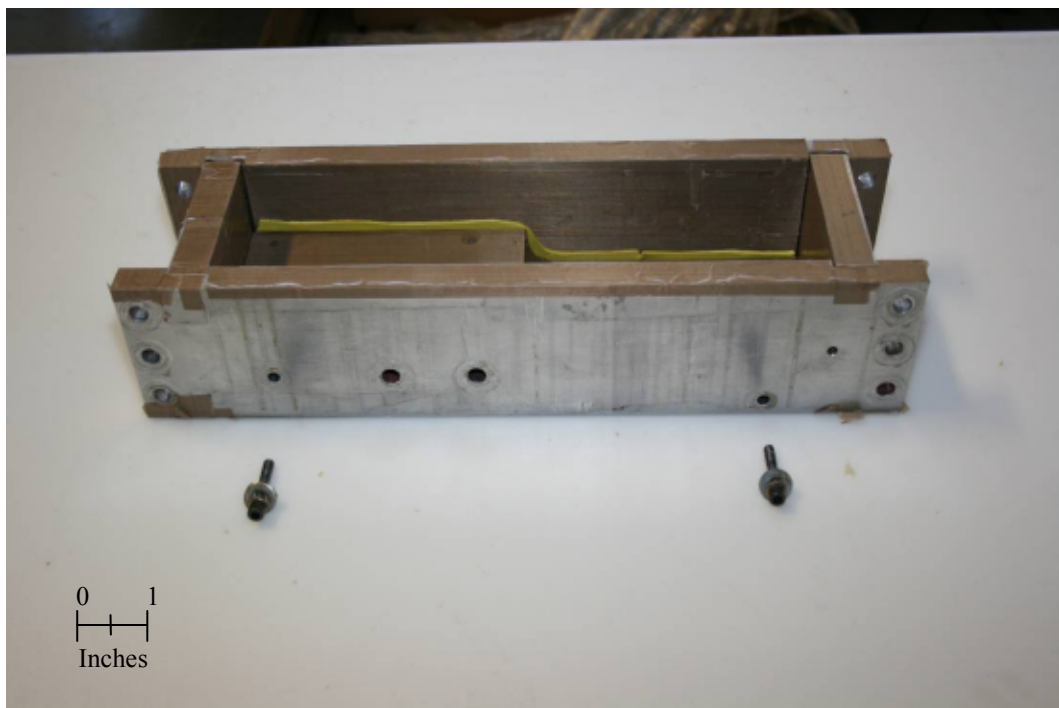


Figure B-4. Properly Positioned Mold Pieces

5. Insert all eight threaded rod pieces into their holes and hand tighten the washers and nuts on both sides of each. Tightening of all threaded fasteners should be done in a balanced fashion such that one end of the mold is not fully tightened while the other is still loose (this would cause unwanted stress and deflections in the mold sidewalls). Figures B-5 and B-6 show the assembled mold. Additional vacuum bag sealing mastic may be placed at inner seam between the mold base and end wall to minimize the amount of resin draining from the mold. The addition of this extra mastic may not be desirable for all brands of pre-impregnated carbon fiber fabric.

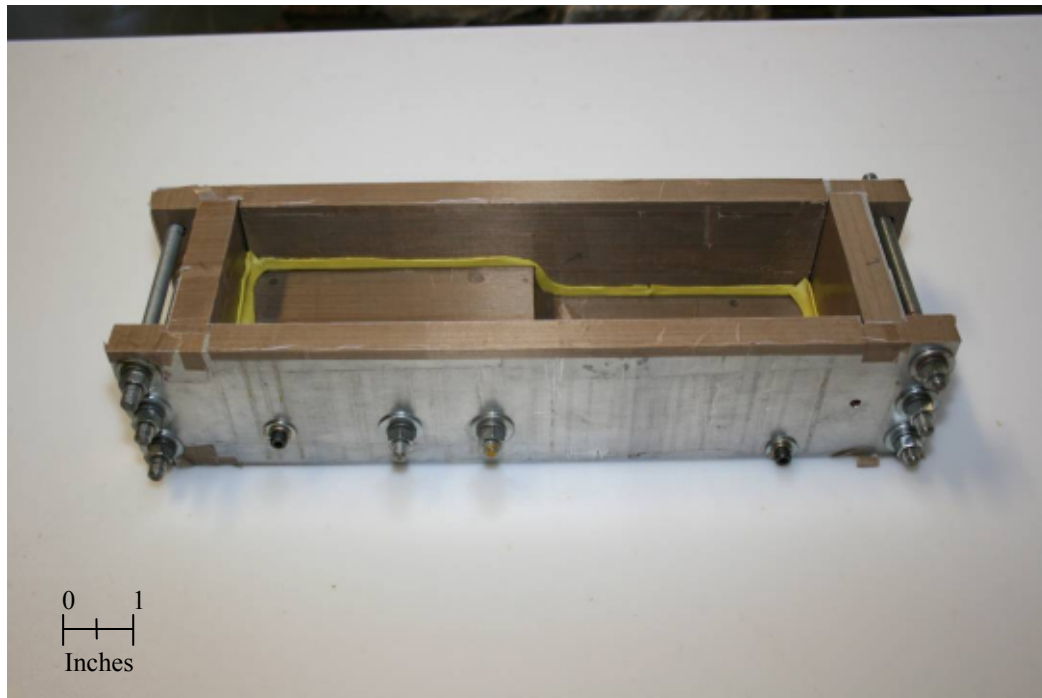


Figure B-5. Assembled and Fully-tightened Mold Body



Figure B-6. View of Mold Body Cavity

6. Begin placement of the carbon fiber strips by laying four of the 6 in. long strip in the lower portion of the mold cavity as shown in Figure B-7. The strips should be placed such that one end rests at the beginning of the step in the mold base.

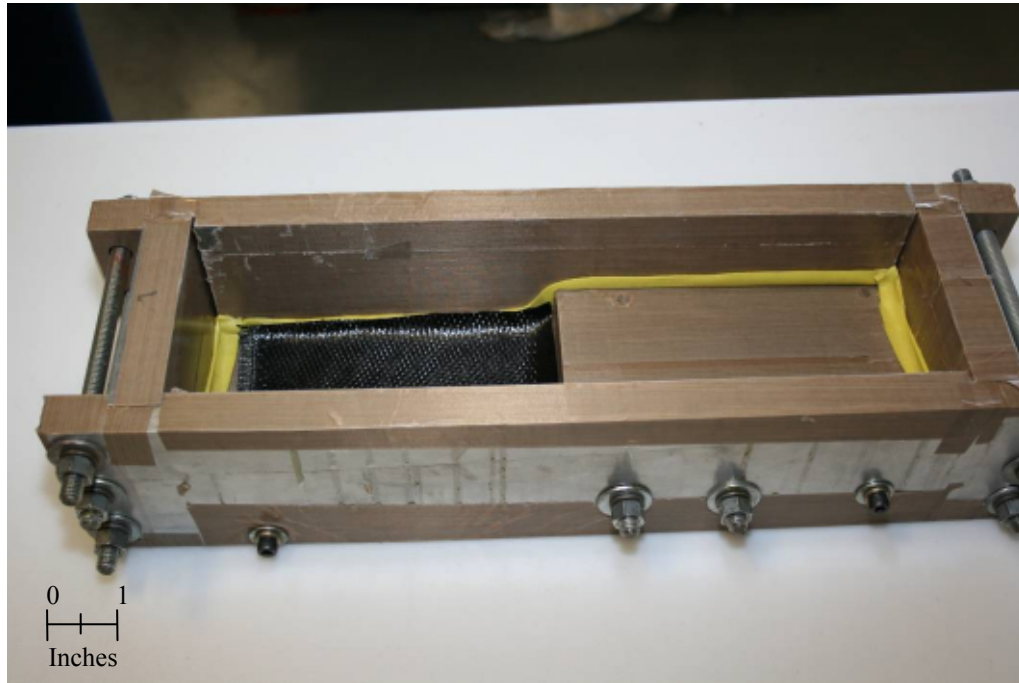


Figure B-7. Placement of 6 in. Carbon Fiber Base Plies

7. Roll the resin film strips into three separate rolls. Place the rolled up 4in. long resin film at one end of the 42 in. long carbon fiber roll. Roll the carbon fiber strip up around the resin film such that the resin film is in the center of the finished roll. Repeat for the 21 in. long carbon fiber roll with one of the remaining resin film rolls at its center. Place the large roll (from the 42 in. strip) at the step in the mold base. Place the smaller roll next to it in the lower portion of the mold cavity. Place the final resin film roll next to and tightly against the smaller roll (Figure B-8).

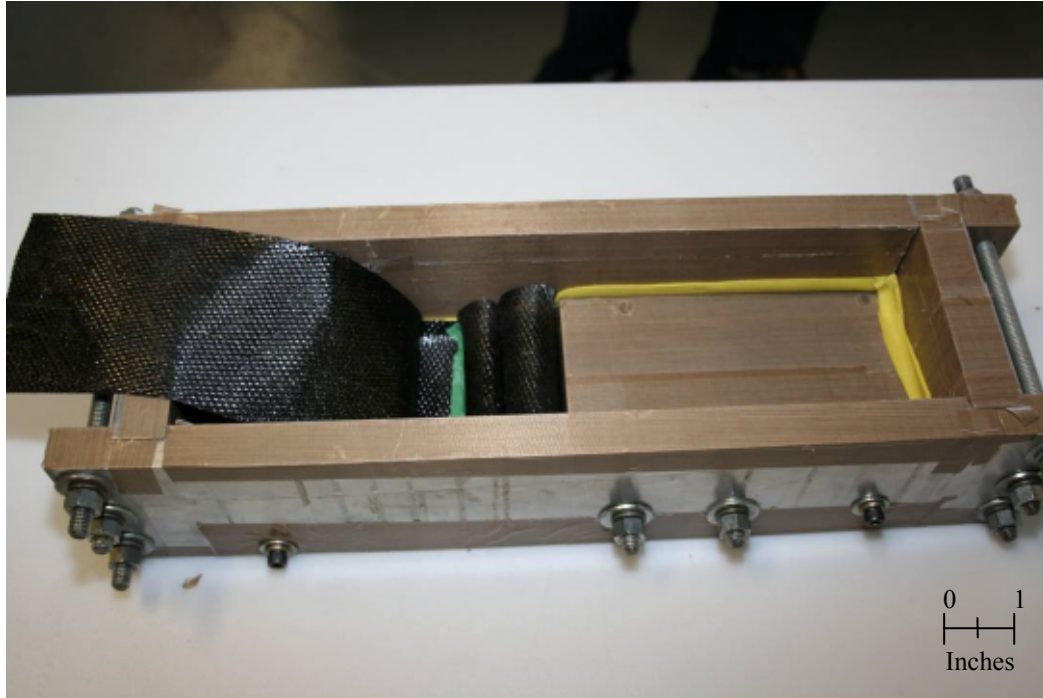


Figure B-8. Placement of Carbon Fiber and Resin Film Rolls

8. Begin laying down the main plies. These plies should start in the lower portion of the mold cavity (Figure B-8) and their end should be spaced a distance of 1 in. from the inner surface of the mold end. Lay the carbon fiber plies in the following order:
 - a. (1) 12 in. long carbon fiber strip
 - b. (1) 11 in. long carbon fiber strip
 - c. (1) 10 in. long carbon fiber strip
 - d. (1) 9 in. long carbon fiber strip
 - e. (1) 8 in. long carbon fiber strip
 - f. (1) 7 in. long carbon fiber strip
 - g. (1) 6 in. long carbon fiber strip
 - h. (1) 11 in. long boron fiber strip (be careful, boron fibers are sharp and give nasty splinters that must be removed immediately!)

Figures B-9 and B-10 show the carbon-fiber and boron plies placed in the mold cavity. The plies should be centered in the mold on top of each other to achieve the curved shape of the overlay.

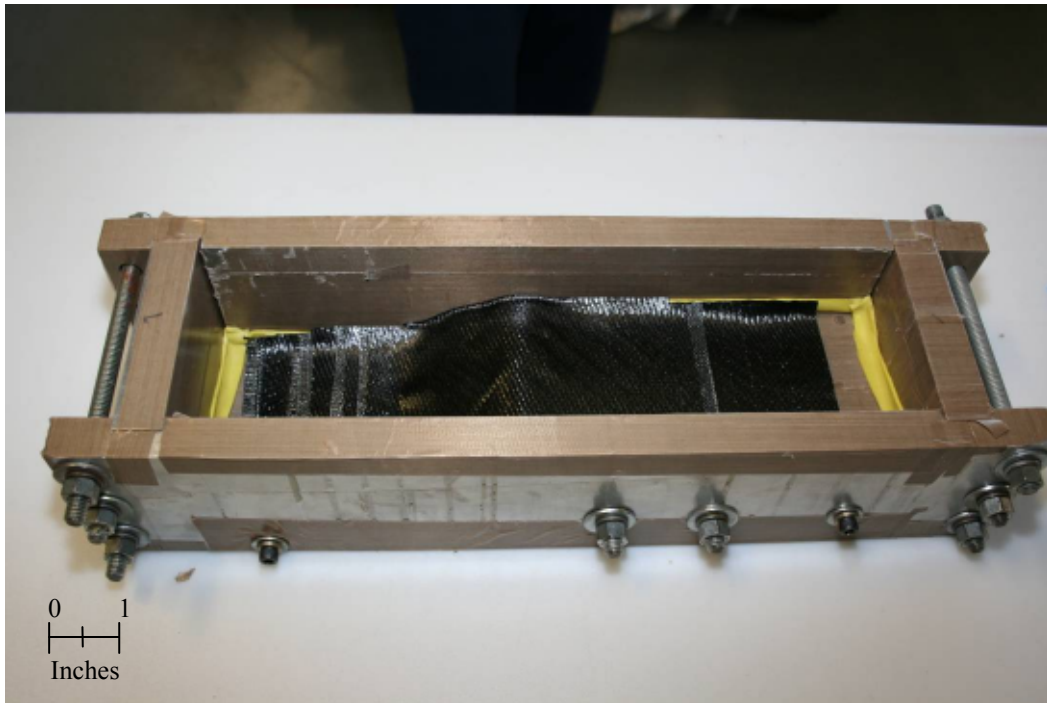


Figure B-9. Placement of Carbon Fiber Plies

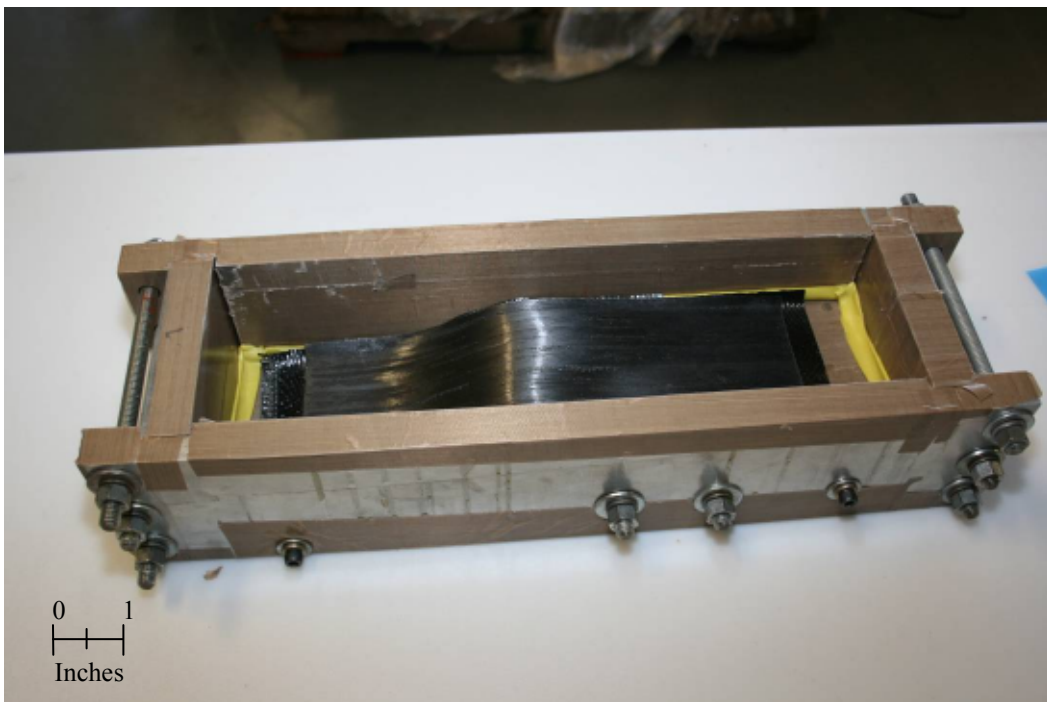


Figure B-10. Placement of Boron Fiber Ply

9. Repeat step 8 three additional times.
10. Place one of the 11 in. long resin film strips on the boron fiber ply in the mold cavity (Figure B-11). The resin film strip should be centered in the mold cavity.

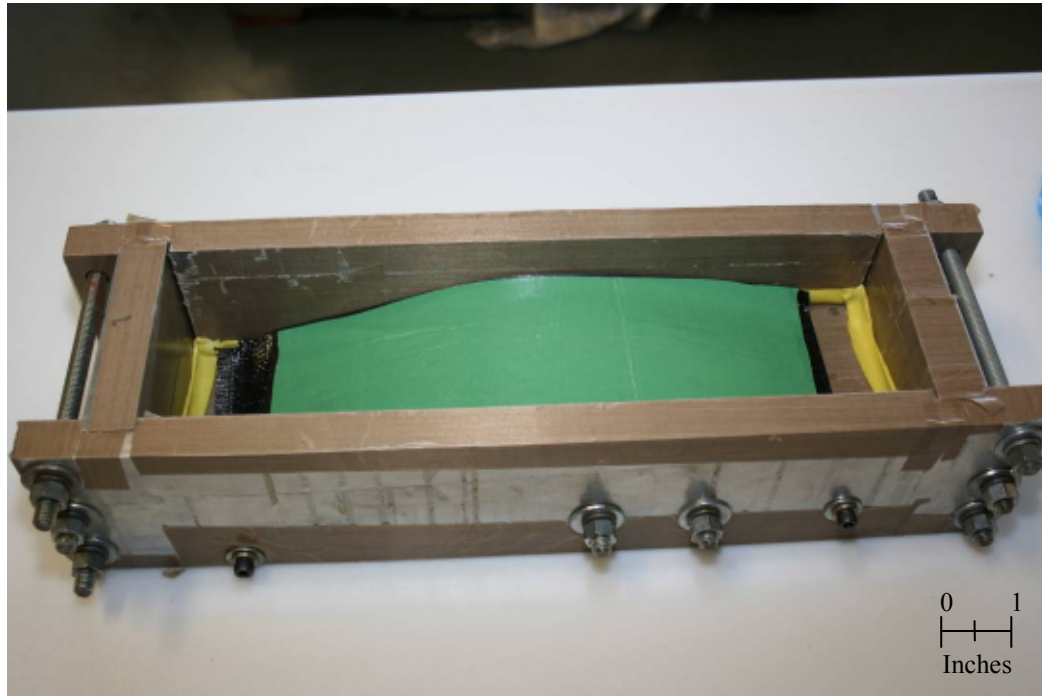


Figure B-11. Placement of Resin Film Strip

11. Repeat step 8 and step 10 one additional time.
12. Lay the remaining 12 in. long carbon fiber strip on the resin film strip. This is the cover ply.
13. Place the former block in the mold cavity such that the shape matches the curvature of the plies (Figure B-12). Position the former block in the mold cavity with the aid of the rubber mallet. The fully positioned former block should be completely within the mold cavity (Figure B-13).

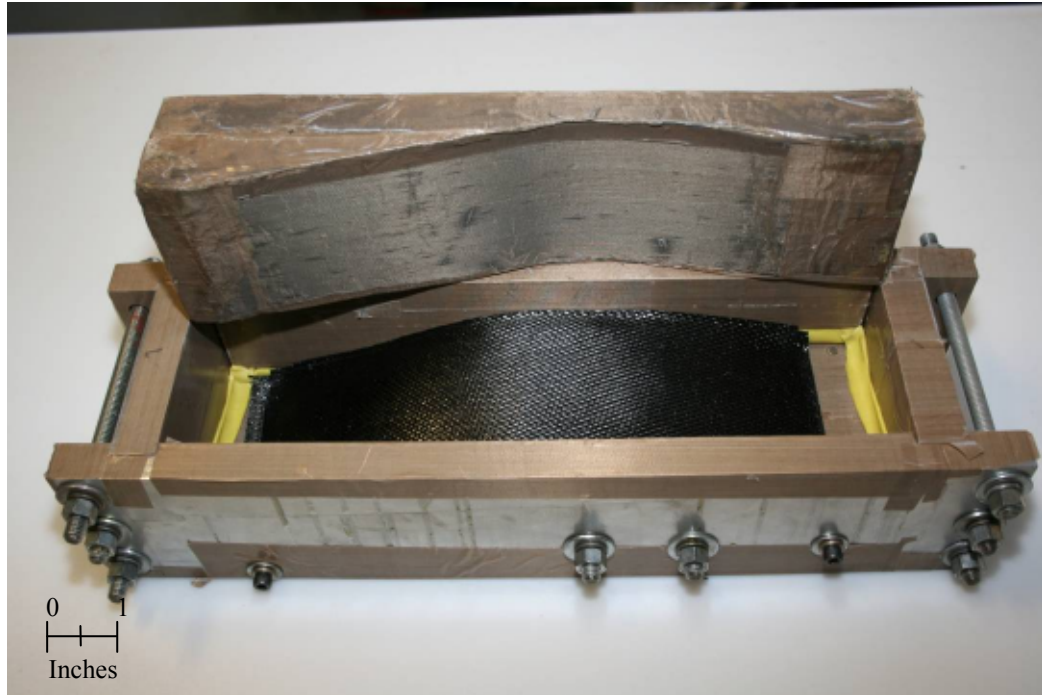


Figure B-12. Mold Body and Former Block



Figure B-13. Former Block Fully Positioned in Mold Body

14. Place mold press plate on top of former block in mold cavity (Figure B-14). Press plate may need to be positioned with the aid of the rubber mallet.

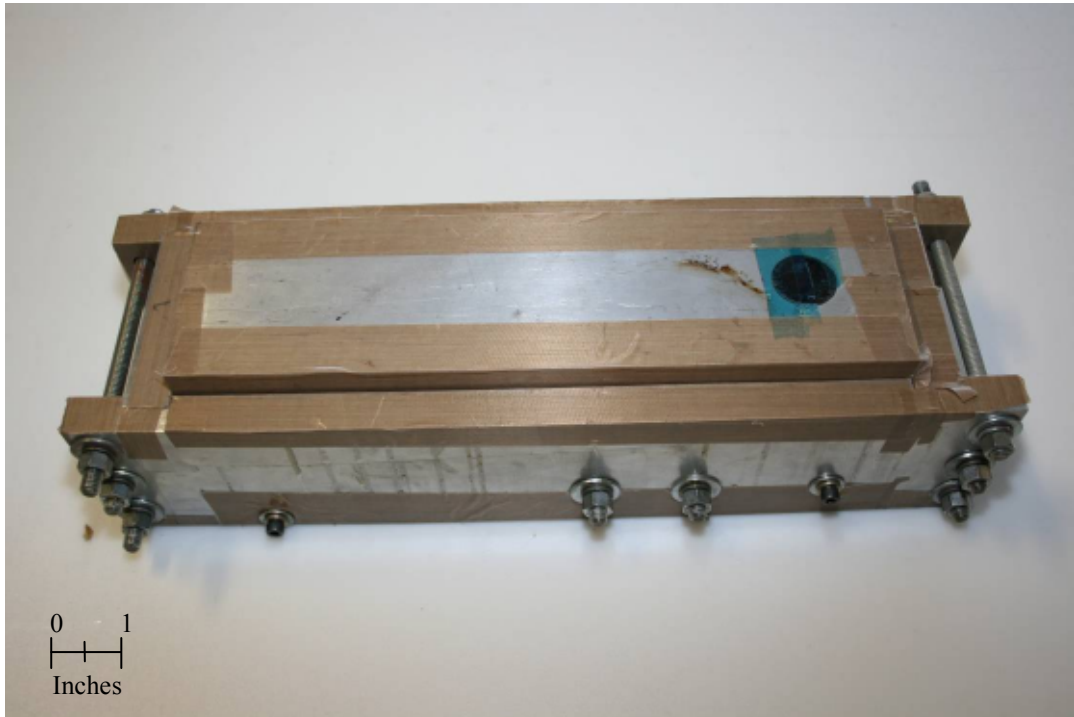


Figure B-14. Press Plate Fully Positioned in Mold Body

15. Place mold into nylon vacuum bag material and seal ends with heat resistant tape. Place on catch pan. Figure B-15 shows the completely assembled mold.



Figure B-15. Fully Assembled Mold

16. Place the assembled mold into the heat press in between the platens (Figure B-16). Follow manufacturer's instructions to apply fourteen tons of load to the mold and heat the platens up to 350 °F (Figure B-17). Leave mold in press under load and temperature for 3-6 hours depending on the time required for the platens to heat up, and the quality of the resin in the carbon fiber fabric.



Figure B-16. Assembled Mold Positioned in Heat Press



Figure B-17. Assembled Mold Subjected to Load and Temperature in Heat Press

17. To ensure resin has achieved cross-linking, test resin that has drained from mold into vacuum bag by attempting to move the bag around resin pool (Be careful, mold and heat press are hot!). If the resin in the pool breaks like hard candy, then the load and temperature may be removed from the mold. It is suggested that the mold be left unloaded in the heat press to cool prior to removal as it will be very hot to the touch.

B1.1.3. POST-PROCESSING OF CFRP OVERLAYS

1. The fully assembled mold should be cool and removed from the heat press prior to this step. Personal protective equipment should be in place. Place catch pan aside. Remove the nylon vacuum bagging material from around the mold and discard. Figure B-18 shows the mold ready to be taken apart.



Figure B-18. Mold Ready to be Taken Apart

2. Loosen the threaded rod and cap screws in a balanced fashion, and set aside (Figure B-19). If any resin or gasket material is found adhered to the threaded fasteners, remove prior to reuse.



Figure B-19. Mold with Threaded Fasteners Removed

3. Using the aid of the rubber mallet, release the sidewalls of the mold (Figure B-20). Next, remove the press plate from the mold. Set these pieces aside for cleaning prior to reuse. Figure B-21 shows the remaining mold pieces with the sidewalls and press plate removed.



Figure B-20. Mold with One Sidewall Released



Figure B-21. Remaining Mold Pieces with Sidewalls and Press Plate Removed

4. Stand the remaining portion of the mold up on one end. Use the rubber mallet to drive a chisel between the mold base and the former block until it has been inserted by at least half of an inch (Figure B-22). By turning the chisel, the mold base and former block will be separated (Figure B-23). Remove the former block and set aside to be cleaned prior to reuse.



Figure B-22. Chisel Driven Between Mold Base and Former Block



Figure B-23. Release of Former Block from Mold Base

5. Use the rubber mallet to drive the chisel between the mold base and the CFRP overlay element (Figure B-24). Be careful not to damage the CFRP overlay element. The mold base and CFRP overlay element should separate with only minimal force. Set the mold base aside to be cleaned prior to reuse.



Figure B-24. Chisel Driven Between Mold Base and CFRP Overlay Element

6. The unmolded CFRP overlay element has ‘fins’ of excess CFRP material protruding from the edges and ‘flaps’ of gasket material adhered to the bottom (Figure B-25). Trim back the gasket material using a razor blade. Trim back the excess CFRP material using shear made for composite materials. The excess CFRP material need only be trimmed to within an eighth of an inch of the CFRP overlay element upper surface. (Be careful when handling the CFRP element to avoid rubbing the surfaces of the composite as boron fibers may be protruding from it, and can cause nasty splinters that must be removed immediately!)



Figure B-25. CFRP Overlay Element Removed from Mold

7. Using a water-cooled tile saw with a diamond blade cut the CFRP overlay element down to achieve a width of three inches (Figure B-26). A cut should be made to each side. Always follow manufacturer's instructions for the safe and proper cutting techniques when using a tile saw. Coolant, usually water, is always required as excess heat can warp or damage the blade, which could lead to serious injury.



Figure B-26. Post-processing of CFRP Overlay Element Sides

8. Using a water-cooled tile saw with a diamond blade, square the ends of the CFRP overlay element such that the thickness of the CFRP material at each end is approximately one eighth of an inch (Figure B-27).



Figure B-27. Post-processing of CFRP Overlay Element Ends

9. Rinse any carbon-fiber cutting residue from the CFRP overlay element, and dry using a towel or paper towels. (Be careful when drying the CFRP overlay element to avoid splinters. Dabbing as opposed to rubbing is recommended.) A fully processed CFRP overlay element is shown in Figure B-28 along with the material that was cut from each side.



Figure B-28. Post-processed CFRP Overlay Element and Removed Material

B1.2 INSTRUCTIONS FOR BONDING OF CFRP OVERLAYS

Bonding of the CFRP overlay elements proved to entail several unique challenges. The epoxy resin being utilized to create the bond had a very low viscosity immediately after mixing. This was essential for the formation of a good bond as it allowed the resin to flow into micropores and cracks on the surfaces being bonded. This propensity for flowing into the every nook and cranny, however, led to most of the molding techniques springing leaks. Ultimately, the best method for reducing leakage during the bond curing time period was to utilize a resin captivation layer in the bond. The resin captivation layer used in this research was a fabric made from randomly oriented polyester fibers. Bonding of the CFRP overlay elements utilizing this resin captivation layer is described here. If a resin captivation layer is not desired, the process is very similar to what is described here, and can be achieved by simply ignoring all mention of that layer (this is not recommended, however, from the standpoint of bond tenacity).

B1.2.1 BONDING OF CFRP OVERLAY ELEMENTS

1. Prepare the surface of the steel to be bonded, personal protective equipment should already be in place. All mill scale and rust must be removed. Since a rough surface finish is adequate, a standard hand grinder was found to be the most efficient method for removing the majority of the mill scale. Special care should be taken in the near vicinity of welds, and use of a dremel with a sandpaper attachment or hand sanding may be required to prepare these areas without gouging the weld. Remove all debris from the grinding process using an isopropyl alcohol moistened rag.
2. Condition the newly prepared surface with a mild acid to break up any grease and oil that may be present (gloves and safety glasses must be worn when handling chemicals). In most cases the acid is applied and allowed to sit on the surface for approximately 5 min. Then, using isopropyl alcohol moistened

paper towels, wipe from one end of the surface to the other in one motion with each towel. Do not reapply the towel to the surface after it has been used.

3. Roughen the surface of the CFRP overlay with 200 grit sandpaper, and remove any debris using isopropyl alcohol. Set aside.
4. Using lengths of vacuum bag sealing mastic, create a barrier around the area where the bond between the steel and CFRP overlay will be created. Allow a minimum of 1/8 in. clearance between the mastic and the sides of the CFRP overlay to eliminate seating difficulties. Leave a minimum of 1/2 in. space between the mastic and the ends of the CFRP overlay to create resin pools at the ends of the bond. When applying the mastic, it is important to use as much pressure as possible. This will give the best possible seal between the steel and the mastic, and between the different lengths of mastic where they join such as corners.
5. Obtain steel ball bearings to be used as spacers to achieve the desired bond thickness. If a very thin bond is desired, steel wire may need to be used instead of ball bearings. If a minimum thickness bond is desired, then no spacer is required.
6. Cut the polyester fiber fabric material to size to act as the resin captivation layer in the bond. The dimensions of the fabric should at the minimum be equal to those of the area to be bonded. For thick bonds, several layers of this fabric may need to be used. Cut a hole in the fabric for each of the ball bearings (a slot is to be cut if steel wire spacers are used). The hole should be just large enough for the ball bearing.
7. Mix the two-part resin epoxy. In this research, Hysol (Loctite #9412) resin was used. It is always best to estimate the volume of the bond prior to mixing the resin-epoxy to give an approximate idea of how much will be required, and it

should go without saying that gloves and safety glasses must be worn when handling chemicals.

8. Begin creating the bond by pouring enough resin into the area within the mastic barrier to achieve a thin layer over the entire area. Spreading the resin with wooden stir sticks is recommended to speed up the process. Place the polyester fiber fabric piece onto this thin layer (if multiple polyester fiber fabric layers will be used, only place one at this time). Place the ball bearings into the holes (or slots for wire spacers). Pour more resin on top of the fabric and allow to soak in. Tamp the fabric with the end of a stir stick until to ensure that the fabric is fully saturated. If required, pour more resin on the fabric. If multiple layers of polyester fabric are being used, place the second layer at this time, and saturate it with the resin in a similar manner as the first. Repeat until all layers have been placed and saturated.
9. Spread a thin layer of the resin on the surfaces of the CFRP overlay to be bonded. Ensuring that the surfaces are completely coated with resin will greatly decrease the potential for void development in the bond.
10. Apply the CFRP overlay to the steel specimen by laying it on top of the saturated polyester fiber fabric layers. Position the CFRP overlay element as desired.
11. Clamp the CFRP overlay to the steel specimen (C-clamps or bar clamps are recommended). The appropriate clamping force is that which can be achieved by tightening the clamps by hand, use of wrenches or torque bars is unnecessary. The clamps should be of sufficient size to apply the clamping force at or near the centerline of the specimen. The specimen must remain level during the curing process, so placement on top of blocks prior to clamping is recommended.
12. Place paper towels underneath the bond area to catch any leaks that may occur. Multiple layers are recommended.

13. For the Hysol resin, a significant increase in viscosity occurs 30 minutes after mixing. At this time, the specimen should be inspected for leaks, and more resin can be added if needed by pouring into the resin pool areas or along the sides of the CFRP overlay. Do not unclamp the CFRP overlay at this time.
14. At room temperature, curing (a high percentage of polymers in the resin developing cross-linking bonds) of the Hysol resin was achieved after 48 hours. The clamps could be removed after 24 hours, but no load was applied until the full cure duration had elapsed.
15. Removal of the vacuum bag mastic material is easiest if the material is stretched as it is being removed. This helps release the material from the steel and resin surfaces.

It should be noted that many different bonding methods were attempted, and the one described above provided the best result both from a bond dimension and bond tenacity perspective. Additionally, one goal of this research was to keep in mind the potential future use of CFRP overlays, and so methods that could be readily used in a field environment were chosen. Alternatively, the resin could be cured much faster in an oven at a higher than room temperature environment. More information on this curing method can be obtained from the resin system specification literature from the manufacturer of the resin system.

APPENDIX C

SUPPLEMENTAL INFORMATION

C1.1 CFRP MATERIAL TESTING

Tensile testing was performed on specimens made from the bi-directional carbon-fiber fabric used to manufacture the CFRP overlays. The aim of this testing was to determine the average modulus of elasticity of the CFRP material, which could be used in the finite element models created to aid the research initiative. The tests were conducted in accordance with ASTM D3039.

C1.1.1 EXPERIMENTAL SETUP

Tensile specimens were created using the bi-directional carbon-fiber fabric (pre-impregnated with cyanamide-123 resin) that was also used to manufacture the CFRP overlays. Each specimen had two plies, and was cured in a heat press at 250 °F for a duration of 5 hours. After cooling, the specimens were cut to dimension using a shear, and the edges were sanded to remove any splintered surfaces. After post processing, thin aluminum plates (tabs) were bonded at the ends to provide better grip performance during the test. Tabbing of the specimen ends is recommended by ASTM D3039 to avoid slippage and damage to the specimen material. Figure C-1 shows a schematic of the specimens.

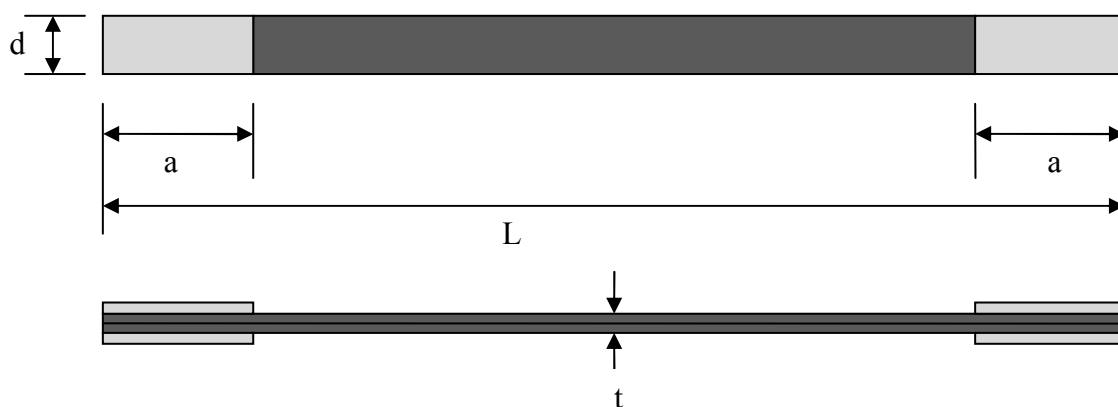


Figure C-1. Schematic of Tensile Test Specimens

The recorded dimensions of the specimens are shown in Table C-1. The depth and the thickness presented in the table are the average of six measurements taken at equal spacing along the length of each specimen.

Table C-1. Test Specimen Dimensions

Specimen	Length, L in.	Tab Length, a in.	Depth, d in.	Thickness, t in.
1	27.1875	1.50	0.774	0.0260
2	27.1875	1.50	0.759	0.0265
3	27.25	1.50	0.742	0.0257

The specimens were tested in tension using an electric drive test frame, Instron model #3345. The test frame controller recorded load and displacement during the test and saved this data to be analyzed. Additionally, several guage marks were made on each specimen at 2 inches above and below the centerline in the event that excessive slippage occurred at the grips. This did not prove to be the case, however, so the guage lines were not ultimately utilized. The load application rate of the test frame was set to 0.5 in./min. as specified in ASTM D3039. Since the purpose of the testing was not to load the specimens to failure, but to simply determine the elastic modulus, the test frame was programmed to stop the test at a static load of 500 lb.

C1.1.2. DISCUSSION OF RESULTS

The load and displacement data recorded during the testing was analyzed to determine the stress vs. strain curves for each specimen. From these curves, the average modulus of elasticity for the elastic portion of the curve (excluding any toe-in region) was determined for each specimen as well as the standard deviation of the modulus of elasticity data. Finally, an average value was determined across the three specimens. The stress vs. strain curves, and average elastic moduli data are shown in Figure C-2. The average modulus of elasticity for the CFRP material tested was determined to be 3,860 ksi.

Stress vs. Strain for Graphite-Epoxy FRP Specimens - 2-Ply, Hot-Press Cured
(Cytac Fiberite P/N: 761252)

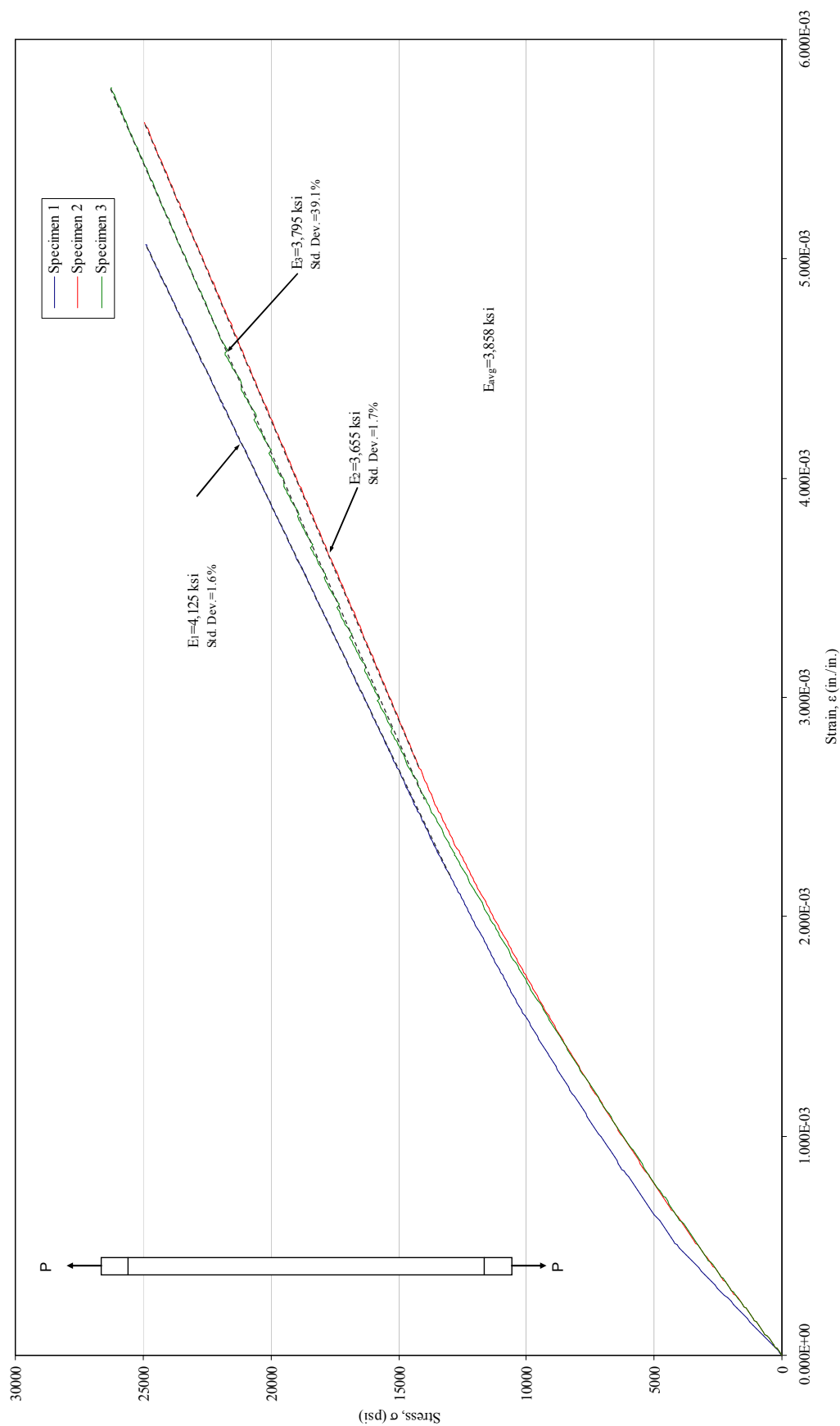


Figure C-2. Stress vs. Strain Curves for Tensile Test Specimens (Max. Load of 500 lb.)